

# 1 Observed slump of sea land breeze in Brisbane under the 2 effect of aerosols from remote transport during 2019 3 Australia mega fire events

4 Lixing Shen<sup>1</sup>, Chuanfeng Zhao<sup>1\*</sup>, Xingchuan Yang<sup>1</sup>, Yikun Yang<sup>1</sup>, Ping Zhou<sup>1</sup>

5 <sup>1</sup>College of Global Change and Earth System Science, and State Key Laboratory of Earth Surface  
6 Processes and Resource Ecology, Beijing Normal University, Beijing 100875, China

7 *Correspondence to:* Chuanfeng Zhao ([czhao@bnu.edu.cn](mailto:czhao@bnu.edu.cn))

8 **Abstract.** The 2019 Australia mega fires were unprecedented considering its intensity and consistency.

9 There have been many researches on the environmental and ecological effects of ~~this~~ mega fires, most

10 of which focused on the effect of huge aerosol loadings and the ecological devastation. Sea land breeze

11 (SLB) is a regional thermodynamic circulation closely related to coastal pollution dispersion yet few

12 have looked into how it is influenced by different types of aerosols transported from either nearby or

13 remote areas. Mega fires provide an optimal scenario of large aerosol ~~emission~~ loadings. Near the coastal

14 site of Brisbane Archerfield during January in 2020 when mega fires were the strongest, reanalysis data

15 from Modern-Era Retrospective analysis for Research and Applications version 2 (MERRA-2) showed

16 that mega fires did release huge amounts of aerosols, making aerosol optical depth (AOD) of total

17 aerosols, ~~b~~Black ~~c~~Carbon (BC) and ~~o~~Organic ~~c~~Carbon (OC) approximately 240%, 425%, 630% of the

18 averages ~~in~~ other non-fire years. Using 20 years' wind observations of hourly time resolution from

19 global observation network managed by National Oceanic and Atmospheric Administration (NOAA),

20 we found that ~~the~~ SLB day number during that month was only four, accounting for 33.3% of the multi-

21 years' average. The land wind (LW) speed and sea wind (SW) speed also decreased by 22.3% and 14.8%

22 compared with their averages respectively. Surprisingly, fire spot and fire radiative power (FRP) analysis

23 showed that heating effect and aerosol emission of the nearby fire spots were not ~~the~~ main causes of local

24 SLB anomaly while the remote transport of aerosols from the fire center was mainly responsible for the

25 decrease of SW, which was partially offset by the heating effect of nearby fire spots and ~~the~~ warming

26 effect of long-range transported BC and CO<sub>2</sub>. The large scale cooling effect of aerosols on sea surface

27 temperature (SST) and the burst of BC contributed to the slump of LW. The remote transport of total

28 aerosols was mainly caused by free diffusion while large scale wind field played a secondary role at 500

29 m. Large scale wind field played a more important role in aerosol transport at 3 km than at 500 m,

30 especially for the gathered smoke, but free diffusion remained the major contributor. The decrease of  
31 SLB speed boosted the local accumulation of aerosols, thus further made SLB speed decrease, forming  
32 a positive feedback mechanism.

### 33 1. Introduction

34 Aerosols play an important role in balancing the Earth's radiation budget, through ~~their~~ direct or  
35 indirect effect (Albrecht, 1989; Garrett and Zhao, 2006; IPCC, 2013; McCoy and Hartmann, 2015). There  
36 are different ~~types~~ kinds of aerosols from various sources which have different climatological forcing  
37 effects (Charlson, 1992; Yang et al., 2016). Aerosols differ in radiative forcing effects as their physical  
38 and chemical properties vary, some of which may affect the earth-atmosphere system by bringing  
39 changes to the lifespan of clouds (Albrecht, 1989; Zhao and Garrett, 2015).

40 Carbonaceous aerosol contains black carbon (BC) and organic carbon (OC) and serves as a major  
41 radiation-influencing aerosol which mainly ~~originates~~ comes from biomass burning (Vermote et al., 2009,  
42 Yang et al., 2021). There have been studies addressing the importance of BC on atmospheric warming  
43 and that of OC on weakening *in situ* downwelling solar radiation (Jacobson, 2001; Ramana et al., 2010).

44 There ~~are~~ were also some studies trying to quantify the average radiative forcing ~~effects~~ of BC and OC  
45 while they ~~also~~ emphasized the potential uncertainties with respect to the specific values ~~too~~ (Zhang et  
46 al., 2017). At a planetary scale, the change of aerosols brings many uncertainties to radiation balance  
47 thus further influences the magnitude of atmospheric circulation (Wang et al., 2015; Zhao et al., 2020).

48 At a synoptic scale, aerosols can affect tropical cyclone by enlarging its rainfall areas which is also related  
49 to ~~their~~ radiative properties (Zhao et al., 2018). At a regional scale, Han et al. (2020) discussed in detail  
50 the radiative forcing effect of aerosols on the speed of Urban Heat Island (UHI) ~~in during~~ different  
51 seasons.

52 As mentioned above, biomass burning is an important source of aerosols, especially for carbonaceous  
53 aerosols. Adequate amounts of fire-emitted aerosols would bring perturbations to the balanced Earth's  
54 climate system through both direct and indirect effects (Jacobson, 2014). There have been many  
55 researches discussing the characteristics of wild fire aerosols and their effect around the world (Grandey  
56 et al., 2016; Mitchell et al., 2006). For example, Portin et al. (2012) investigated the characterization of  
57 burning aerosols in Eastern Finland during Russian wild fires in ~~the summer of~~ 2010. Kloss et al. (2014)

58 pointed out ~~that~~ wild fires could ~~bring~~ have plumes ~~of smoke that~~ ascend ~~very~~ high and pollute~~ing~~  
59 remote areas with the help of monsoon. Grandey et al. (2016) quantified the ~~total fire aerosol~~ radiative  
60 effect ~~of the total fire-induced aerosols~~ over the globe, which ~~was~~ estimated to be  $-1.0 \text{ W/m}^2$  on average.  
61 The fire-~~induced~~ aerosols could have more significant radiative effects with clouds than under clear sky  
62 condition through cloud-aerosol interaction, whose global forcing effect could reach  $-1.16 \text{ W/m}^2$   
63 (Chuang et al., 2002).

64 Australia is one of the areas where wild fires occur frequently (Yang et al., 2021). There are nearly  
65  $550,000 \text{ km}^2$  of tropical and arid savanna~~s~~ burnt each year in Australia, contributing to about 6%–8%  
66 of global carbon emissions from biomass burning (van der Werf et al., 2006; Meyer et al., 2008).  
67 Particularly, there have been many studies concentrating on wild fires' association with enhancing  
68 aerosol loadings and air pollution events in Australia, some of which included the discussion ~~one~~ of the  
69 combined effect from background meteorological conditions (Mitchell et al., 2006; Luhar et al., 2008;  
70 Meyer et al., 2008; Mitchell et al., 2013; Mallet et al., 2017). The 2019 Australia wild fires from  
71 December 2019 to February 2020 were unprecedented in recent decades in terms of ~~the~~ magnitude and  
72 consistency so that they have attracted the attention of the world in a short time. ~~Since their outbreak,~~  
73 ~~n~~ ~~numerous~~ studies have been carried out ~~to investigate them~~ ~~since their outbreak~~ from different  
74 aspects. For example, Yang et al (2021) examined the statistical properties of aerosol properties  
75 associated with 2019 Australia mega fire events in both horizontal and vertical directions. Torres et al.  
76 (2020) investigated the aerosol emissions during the mega fires happening in New South Wales, Australia  
77 and found a great amount of carbonaceous aerosols in the stratosphere. Ohneiser et al. (2020) traced  
78 wildfire smoke in one of the most severe burnt areas in southeastern Australia and found that smoke  
79 could even travel across the Pacific, which was detected by an observation site at Punta Arenas in South  
80 America.

81 Sea land breeze (SLB) is a common circulation over coastal areas whose direct cause is the ~~regional~~  
82 temperature difference between land and sea (TDLS). Many studies have investigated this regional  
83 circulation. On one hand, the complicated influencing factors of SLB have been studied from different  
84 perspectives (Miller et al., 2013). Our previous studies pointed out that the change of TDLS is highly  
85 related to the change of *in situ* downwelling solar radiation (Shen et al., 2021 ~~a, b~~; ~~Shen et al., 2021~~; Shen  
86 and Zhao, 2020). We also found that the continuous increase of surface roughness in cities ~~can~~ reduce  
87 the SLB speed in long term (Shen et al., 2019). The long-term significance and trends of SLBs over the

88 globe are driven by climate regimes which are related to climatological differences in both *in situ*  
89 downwelling solar radiation and background wind fields. There are also many other studies on the  
90 influencing factors of SLB ~~induring~~ short periods. For example, based on the case analysyses, Sarker  
91 et al. (1998) found that UHI magnitude has a great impact on the encroachment range of sea wind (SW)  
92 frontal surface. Using regional model simulation, Ma et al. (2013) found that UHI effect ~~can~~ greatly  
93 enhance TDLS ~~a lot~~ which would result in strengthened SLB circulation in a great metropolis. Miller et  
94 al. (2013) reviewed the studies on SLB and pointed out that local topography such as the shape of the  
95 coastline, is another important influencing factor of SLB. On the other hand, SLB's effect has also been  
96 extensively investigated. For example, SLB has been reported as a direct controller of air pollutants  
97 which transports air pollutants inland or to the vast ocean with the help of background meteorological  
98 field (Nai et al., 2018; Shen and Zhao, 2020). SLB is also essential to the modification of the  
99 meteorological conditions and local climate (Rajib and Heekwa, 2010). Moreover, SLB is a determinant  
100 factor of the diurnal variation of the precipitation on the island since its direction and magnitude can  
101 affect the location and magnitude of convective systems (Zhu et al., 2017).

102 Over the years, the cause and effect of aerosols, wild fires in typical areas, and SLBs have been learned  
103 in detail respectively. The relationship between aerosols and other small scale circulations such as UHI  
104 circulation has also been investigated from many aspects (Han et al. 2020). However, few studies have  
105 investigated the effects of different types of aerosols on SLBs or looked into how local and remote aerosol  
106 ~~emissionsloadings~~ during mega fires would affect local SLB with the help of meteorological background  
107 field or other potential mechanisms. There was an updated and important study calling for attention of  
108 the record-breaking aerosol ~~emissionsloadings~~ during 2019 Australia mega fires which led to significant  
109 cooling effect ~~on~~ ocean temperature (Hirsch and Koren, 2021). Since *in situ* downwelling solar  
110 radiation and SST, which are both important influential factors of SLB, are deeply affected by ~~the~~  
111 ~~radiative effects of~~ different types of aerosols due to their different radiative properties, it is interesting  
112 to examine in detail how the record-breaking mega fires would influence SLB by releasing large amounts  
113 of aerosols.

114 The paper is organized as follows. Section 2 describes the observation site, data and analysis methods.  
115 Section 3 illustrates the characteristics of SLB, the variation of SLB days, the distribution and fire  
116 radiative power (FRP) of wild fire spots, the anomaly of observed SW speed, land wind (LW) speed and  
117 air temperature, the effects of different aerosols on SLB's variation, the analysis on background wind

118 field and the comparison between local fire spots' and the remote fire center'-s contributions. Section 4  
119 summarizes and discusses the findings of the study and proposes a mechanism of aerosol-SLB interaction  
120 during the peak of 2019 Australia mega fires<sup>2</sup>~~most intense period~~.

## 121 2. Data and methods~~Data and methods~~

### 122 2.1 Site

123 The 2019 Australia mega fires occurred mainly in the eastern and southeastern coastal areas of Australian  
124 continent (Yang et al., 2021). The southeastern parts, including the State of Victoria and southeastern part  
125 of the State of New South Wales, belong to Marine Climate where obvious existence of SLB (OE-SLB)  
126 is not clearly verified because of the influence of strong westerlies and water vapor accompanied with  
127 westerlies from the ocean (Shen et al., 2021). Note that OE-SLB means that SLB is significant from a  
128 climatological perspective. In other words, the SLB can be found during most time of the year. Details  
129 ~~of about~~ the definition of OE-SLB can be found in Shen et al. (2021) and are not repeated here. Meanwhile,  
130 the wild fire events there were the most severe with a great density according to numerous reports, which  
131 could possibly cause fire-induced complex flows and circulation in the form of fire-atmosphere  
132 interactions in the vicinity of a fire (Stageberg, 2018). Based on previous observation during mega fire  
133 events, the concentrated fire spots changed the local air pressure field and added a regional temperature-  
134 pressure field, bringing uncertainties to local wind speed and wind direction (Jia et al., 1987; Li et al.,  
135 2016). On one hand, this could further interrupt ~~the~~the SLB formation of SLB since it might make the  
136 background wind field more complicated. On the other hand, the detected SLB might not be accurate  
137 since it is likely to contain other wind disturbance at a small regional scale.

138 As shown in Fig. 1, we selected an urban site in Brisbane along the eastern coast of Australia as the study  
139 site, which was due to several considerations. First, ~~alongside~~while the eastern coastals areas of Australia  
140 which belong to monsoon climate, including Brisbane and areas to its south but to the north of the fire  
141 center, the Australian monsoon system is not strong so that the OE-SLB can be verified from a  
142 climatological perspective, which also means integrated SLB circulation can be found during all seasons.  
143 Second, compared to rural sites, there are longer periodss of high time resolution observation data at urban  
144 sites, which is necessary for the extraction of SLB signals. Third, the urban area of Brisbane is relatively  
145 small and is not very far from vast areas of forests which provide stable combustion environment,

146 ensuring the persistent effect of wild fires ~~when they occur~~. Fourth, the UHI effect, which could possibly  
147 interrupt SLB and bring errors when calculating SLB magnitude, should be small for the study region  
148 considering the small scale of urban areas. Also, the wild fires near suburban areas could further eliminate  
149 the UHI effect even if it could exist through their heating impact on these areas. In contrast, the forest  
150 site is surrounded by or within great amounts of flora where ~~thea~~ majority of solar radiation is absorbed  
151 and scattered by leaves, prohibiting the surface heating by solar radiation and then the formation and  
152 detection of SLB. Actually, due to the existence of photosynthesis, the ~~endothermic heat absorption~~  
153 process of leaves from solar radiation and the temperature rise of 'leave surface' are different from those  
154 of Earth surface. As a result, the traditional mechanism of SLB formation is not necessarily applicable  
155 when the site is in the forest or quite close to clusters of flora. Coastal sites to the north of Brisbane are  
156 too far from the fire center, and they are mostly rural sites covered with flora as well. Considering all of  
157 these, we chose the site of Brisbane Archerfield located at eastern coast of Queensland State (Fig. 1) as  
158 the study site.

## 159 2.2 Data

160 ~~The~~ Several types of data have been used in this study, including the land cover type data, the Modern-  
161 Era Retrospective analysis for Research and Applications version 2 (MERRA-2) data, the Moderate  
162 Resolution Imaging Spectroradiometer (MODIS) data, the ground site observation data, the Fifth Version  
163 of European Centre for Medium-Range Weather Forecasts (ECMWF) ReAnalysis (ERA5) data, the  
164 Firespot and FRP data, and the Global Data Assimilation System (~~GDAAS~~) data. The detailed data  
165 information is described below one by one.

166 Land cover type data: The land cover type data of Australia is from Dynamic Land Cover Dataset (DLCD)  
167 with Version 2.1 provided by Geoscience Australia. In this study, the DLCD land cover type data was  
168 used to reveal the surrounding landscape of Brisbane Archerfield. The spatial resolution of the data is  
169 ' $0.002349^{\circ} \times 0.002349^{\circ}$ ', which is based on the annual mean of ~~satellite observation data~~ from 2014 to  
170 2015.

171 MERRA-2 data: MERRA-2 belongs to the global atmospheric reanalysis product managed by National  
172 Aeronautics and Space Administration (NASA). It is produced by the Global Modeling and Assimilation  
173 Office (GMAO) and the assimilation system of Goddard Earth Observing System (GEOS-5) is used to  
174 ensure the quality of this dataset. ~~At For~~ major ground sites over Australia, Yang et al. (2021) compared

175 its monthly aerosol optical depth (AOD) product with Aerosol Robotic Network (AERONET)  
176 observations and found their RMSEs were all smaller than 0.05. Thus, MERRA-2 should be reliable to  
177 be used for the analysis of the large-scale spatial distribution of AOD in Australia. Yang et al. (2021) also  
178 denoted that the 2019 Australia mega fires were the strongest in January of 2020. Correspondingly, we  
179 used the monthly AOD ~~in~~ January at 550 nm from 2002 to 2020 to check the AOD difference between  
180 the mega fire year and years with no mega fires. The spatial resolution of MERRA-2 AOD data is '0.625°  
181 ×1°'.

182 MODIS data: The MODIS instrument is performed on Aqua and Terra platforms. In this study, we used  
183 the MODIS cloud product which belongs to the dataset of MCD06COSP\_M3\_MODIS. The cloud  
184 information includes cloud optical depth (COD) and cloud fraction for all January months during the  
185 period from 2003 to 2020 with monthly time resolution. The Brisbane Archerfield site is located at  
186 '153.008°E, 27.57°S'. So we used COD and cloud fraction data whose space range and resolution are  
187 '152.5°E-153.5°E×28.5°S-26.5°S' and '1°×1°' respectively. This space range covers the whole Brisbane  
188 area and the normal encroaching distances of SLB which ~~is~~ are about dozens of kilometers (Rajib and  
189 Heekwa, 2010; Shen et al., 2019). In this study, the spatial averages of them were calculated to represent  
190 the local COD and cloud fraction ~~in~~ during every January from 2003 to 2020. Also, we used the MODIS  
191 monthly AOD product to compare with that of MERRA-2, which belongs to the dataset of MOD08\_M3.  
192 The spatial resolution of MODIS AOD data is '1°×1°' and the time range is the same as that of MERRA-  
193 2.

194 Ground site observation data: The wind and air temperature observation data are from National Oceanic  
195 and Atmospheric Administration (NOAA) global observation network at the site of Brisbane Archerfield  
196 (153.008°E, 27.57°S). We used data in January from 2001 to 2020 in this study. The time resolution is  
197 every 3 hours at 200, 500, 800, 1100, 1400, 1700, 2000, 2300 UTC on most days. The continuity of the  
198 observation data is ensured, there are observations on each day in January throughout the whole study  
199 period, with only one missing observation data at each day of a small fraction time (approximately 3.5%).

200 The wind information includes wind speed and wind direction ~~with few missing observations~~. The air  
201 temperature is measured in Fahrenheit and we have converted it into Celsius. The observation data was  
202 the main data used in this study to show the variations of both SLB and air temperature during the fire.

203 ERA5 data: The monthly mean Uwind (zonal) speed and Vwind (meridional) speed ~~in~~ January of 2020  
204 from the ERA5 were used in this study to reveal the background meteorological field so as to assess its

205 effect on aerosol transport. The spatial resolution is ‘ $0.250^{\circ} \times 0.250^{\circ}$ ’ at pressure levels of 1000 hPa, 975  
206 hPa, 950 hPa, 925 hPa, 900 hPa, 875 hPa, 850 hPa, 825 hPa, 800 hPa, 775 hPa, 750 hPa and 700 hPa.

207 Firespot and FRP data: Firespot and FRP data are from MODIS product (MCD14). It can catch and locate  
208 the active fire hotspots based on thermal anomalies of 1 km pixel resolution (Giglio et al., 2016). The  
209 time resolution is daily and we used the monthly averages for January from 2002 to 2020 to look into the  
210 fire situations over the years in detail.

211 GDAS data: The GDAS data was used to perform the back-trajectory analysis from the Hybrid  
212 Single-Particle Lagrangian Integrated Trajectory (HYSPLIT). The spatial resolution of GDAS data  
213 is ‘ $1^{\circ} \times 1^{\circ}$ ’ with daily time resolution. The levels of GDAS data chosen in this study to help to perform  
214 HYSPLIT analysis were 500 m and 3 km respectively. The time range set in this study was the whole  
215 January of 2020.

## 216 **2.3 Methods**

### 217 **2.3.1 Extracting SLB signal**

218 The verification of OE-SLB and extracting of SLB signals from original wind observation over monsoon  
219 areas were carried out through the method of Separation of Regional Wind Field (SRWF). The definition  
220 of OE-SLB, the details of SRWF method and criterion for verification were detailed in our previous  
221 studies and not repeated here (Shen et al., 2019; Shen and Zhao, 2020; Shen et al., 2021). Briefly speaking,  
222 SRWF calculates the vector difference between observed wind vector and daily average wind vector for  
223 each observation time. Then, the vector difference is considered as the local wind. The criterion of OE-  
224 SLB requires that there exist intersection sets among the range of SW, the range of LW and the range of  
225 hourly average of wind angle in a diurnal period (HAWADP). Also, the intersection set between the range  
226 of SW (LW) and the range of HAWADP only exists during daytime (nighttime). Then the local wind can  
227 be thought as the SLB signal as long as the OE-SLB is verified at that site. Based on HAWADP and  
228 specific sea-land distribution, we further defined the prevailing time of sea wind (PTS) and prevailing  
229 time of land wind (PTL). Briefly speaking, during PTS (PTL) the local wind keeps blowing from sea  
230 (land) and the wind angle keeps rotating towards the direction of vast sea (inland). The HAWADP at  
231 Brisbane Archerfield is shown in Fig. 2. As shown, the HAWADP of local wind was close to sinusoid,  
232 which conformed to previous findings in other monsoon areas (Shen et al., 2021; Yan and Anthes, 1987).  
233 According to the sea-land distribution shown in Fig. 1, we first defined the ranges of SW and LW and

234 then the OE-SLB of Brisbane Archerfield was verified using these criteria. We further selected the PTS  
235 (PTL) based on the rules above.

236 To make it clear, we summarized the range of SW, LW, PTS and PTL in Table 1. The ranges of SW and  
237 LW refer to specific sea-land distribution. Notably, there are few mountains within the ranges of SW and  
238 LW based on the accurate site location and detailed landscape nearby, which helps to exclude potential  
239 interruption from other small scale circulation like mountain-valley wind. Note that the actual PTS (PTL)  
240 may be longer than what we defined here because the time resolution is 3 hours instead of hourly in this  
241 study. As a result, we cannot know the exact threshold of time when the wind angle meets the criteria  
242 mentioned above. For instance, it is possible that the wind angle is within the range of SW before 0500  
243 UTC. However, it is still sure that the SW (LW) develops vigorously during 0500-0800 UTC (1400-2000  
244 UTC) based on Fig. 2, which means that ‘0500-0800 UTC’ and ‘1400-2000 UTC’ are within the real PTS  
245 and PTL respectively even if they are not the exact PTS or PTL. Thus, the defined PTS (PTL) in this  
246 study is reliable. The aim to define PTS (PTL) is to find the time period when SW (LW) develops most  
247 vigorously so as to ensure further exclusion of winds from synoptic scales when trying to extract real  
248 SLB signals after applying the SRWF method (Shen and Zhao, 2020; Shen et al., 2021; Cuxart et al.,  
249 2014).

### 250 **2.3.2 Definition of the SLB day**

251 SLB day is the day when SLB circulation is most significant (Xue et al., 1995). To some extent, the  
252 number of SLB days reveals the activity level of SLB. Different criteria have been adopted when defining  
253 SLB day. Here we referred to our previous study (Shen et al., 2019) to adopt the criteria based on the  
254 minimum times of successful detection of winds coming from the range of SW (LW) during PTS (PTL).  
255 Since the time interval between two adjacent observations is 3 hours, which makes the number of total  
256 observation times-hours less than the total hours during prevailing time, we modified the criteria slightly  
257 as follows: when the offshore land winds occur in the time-period of 1400-2000 UTC with total  
258 occurrence time no less than 3, and the onshore sea winds occur in the time period of 500-800 UTC with  
259 total occurrence time no less than 2, the day is counted as a SLB day.

### 260 **2.3.3 The calculation of monthly SW and LW speeds**

261 After defining PTS, PTL and SLB day, we could finally calculate the monthly SW and LW speeds. First,

262 we picked up SLB days in every January from 2001 to 2020. Second, we picked up local wind speed  
263 during PTS (PTL) on SLB days and calculated the monthly average of SW (LW) speed in every January  
264 from 2001 to 2020.

265 Based on GDAS data throughout the whole January in 2020, the back trajectories of lower atmosphere  
266 at Brisbane Archerfield were simulated using the HYSPLIT model, ~~which~~ This could help analyze the  
267 ~~transport~~ effect of background wind fields on aerosol transports \_at this site. The simulated levels at the  
268 site were 500 m and 3 km since the lower level of atmosphere (500m) was closer to fire spots and there  
269 was also accumulated smoke at 3 km in the southeastern parts of Australia during the exact same month  
270 (Yang et al., 2021). The TrajStat module of Meteoinfo version 2.4.1 was also used to cluster the back  
271 trajectories based on the Euclidean distance method, whose details and source code could be found at its  
272 official website (<http://meteothink.org/docs/trajstat/index.html>, last access: 31 January 2021).

### 273 **2.3.4 The calculation of monthly temperature during daytime and nighttime**

274 After defining the SLB day, PTS and PTL, we calculated the monthly mean temperature during daytime  
275 and nighttime using the similar method as SW and LW speeds. First we selected the temperature on SLB  
276 days. Second, we calculated the monthly average of temperature during PTS (PTL) to represent monthly  
277 average temperature during daytime (nighttime) in January. Actually, temperature during daytime  
278 (nighttime) represents land temperature when SW (LW) prevails. In order to make it clear and concise,  
279 we call it temperature during PTS (PTL) or land temperature during daytime (nighttime) in this study.

## 280 **2. Results**

### 281 **3.1 The variation of SLB day number**

282 Figure 3 shows the SLB day number in January from 2001 to 2020. As shown, the SLB day number in  
283 January was normally larger than 10. Among these 20 years, there were 25% of the years whose SLB  
284 days in January accounted for more than half of the month. Note that it does not necessarily mean that  
285 there is no SLB on days that are not SLB days. It is obvious that there was a slump in the number of SLB  
286 day in 2020. The total SLB day number dropped to only 4 during ~~the mega fires~~ events, accounting for  
287 only 33.33% of the average SLB day number during the past 20 years. Also, year 2012 also witnessed  
288 low SLB day number (6 days) in January. There are a lot of potential influencing factors for SLB  
289 frequency, such as the background wind field (Miller et al., 2013) and the interruption of other small

290 scale circulations (Kusaka et al., 2000). Among all the influencing factors, cloud is one of the most  
291 important because it has significant effect on *in situ* solar radiation which is the direct cause of TDLS.  
292 We would discuss this in the following sections.

### 293 3.2 The trends in SW and LW speeds and local air temperature

294 The monthly mean SW and LW speeds in January ~~from 2001 to 2020~~ are shown in Figure 4a. As can be  
295 seen, there were fluctuations ~~in the trends of~~ both SW and LW speeds ~~in January from 2001 to 2020~~.

296 The SW speed was higher than LW speed, which conformed to many previous findings (Miller et al.,  
297 2013; Zhu et al., 2017). The averages were calculated as 3.70 m/s for SW speed and 2.86 m/s for LW  
298 speed, ~~respectively~~~~respectively~~. Figure 4b and c show the anomalies ~~off~~ both SW and LW speeds. In  
299 general, LW speed fluctuated more significantly than SW speed did. This is due to its lower level of  
300 kinetic energy which ~~cannot~~ make it more sensitive to any potential interruptions from the background  
301 meteorological field (Shen and Zhao, 2020). The negative anomalies of LW speed happened in 2001,  
302 2004, 2008, 2010, 2011, 2015, 2016, 2017, 2018 and 2020. Different from other years, it is obvious that  
303 the negative anomaly in 2020 was higher than 0.6 m/s, which was beyond ~~the~~ multi-years' oscillation  
304 range. The anomaly accounted for 22.3% of multi-years' average LW speed. The negative anomalies of  
305 SW speed happened in 2004, 2008, 2009, 2010, 2011, 2013, 2014, 2015, 2017 and 2020 (Figure 4c). For  
306 SW speed, the negative anomaly ~~value~~ in 2020 was also obvious but its ~~value~~ was still within the multi-  
307 year oscillation range. It was higher than 0.5 m/s, accounting for 14.8% of the multi-years' average. It is  
308 interesting to find that there were obvious positive anomalies of both SW and LW speeds in 2003 whereas  
309 their absolute values were not the highest. Also, the SLB day number in 2003 was near the average. We  
310 will further discuss this along with the aerosol emissions during that year in the following sections.

311 It can be seen in Figure 4b that there were also significant fluctuations in nighttime land temperature  
312 over the years. There was a soar in land temperature ~~during nighttime~~ in 2020 which approached nearly  
313 24 °C. It was nearly 3 °C ~~higher~~~~more~~ than the multi-years' average, exceeding the range of multi-years'  
314 oscillation. The fluctuation ~~in~~ land temperature during daytime was less significant than that during  
315 nighttime. There was obvious positive anomaly in 2020, indicating that the daytime land temperature  
316 was higher than those in normal years. Meanwhile, it was still within the range of multi-years' oscillation  
317 ~~range~~ though the positive anomaly was obvious. Fire spots have heating effect on the nearby environment  
318 through either shortwave radiation of light from fires or heat conduction caused by temperature gradient.

319 It can be inferred that mega wild fires ~~in~~during January ~~of~~ 2020 contributed to the positive temperature  
320 anomalies during PTS (PTL) through the heating effect of fires though it might not be the only cause.

321 The heating effect during ~~mega fires~~fire events was more significant during nighttime than ~~during~~  
322 daytime, ~~which~~. This is probably due to colder background temperature field during nighttime.

323 Basically, the decreased SW (LW) speed revealed that the TDLS during PTS (PTL) decreased. To be  
324 more specific, the temperature difference between the small regions where the upward stream and  
325 downward stream of SLB circulation lie respectively became smaller during January ~~in~~ 2020. Based on  
326 Figure 4b and c, temperature during PTL seems to be generally negatively related to LW speed anomaly  
327 while it is obvious that temperature during PTS does not show any corresponding relationship with SW  
328 anomaly.

329 In order to be more accurate, we carried out linear regression between temperature during PTL and LW  
330 anomaly and found that they had negative linear relationship ( $p < 0.02$ ) with each other (Figure 5). As the  
331 temperature increased by 10 °C, the LW speed anomaly decreased by 1.52 m/s. The correlation  
332 coefficient R was 0.52, which was at the medium level. However, considering the significance level as  
333 well as low level of sample number, it can be concluded that the LW speed is generally negatively  
334 correlated with nighttime land temperature. Moreover, their R and significance level could be 0.69 and  
335 0.0012 respectively if we excluded the only one abnormal point in 2019, which might be caused by some  
336 potential disturbances on coastal SST where the vertical stream of SLB lies, either of these two variables.  
337 Considering all these, it can be concluded that the LW speed anomaly is generally negatively correlated  
338 with nighttime land temperature. During nighttime, the land is colder than the sea. As the land  
339 temperature increases, the TDLS ~~decreases~~ ~~becomes~~ ~~smaller~~ if the SST of the area where the upward  
340 stream of SLB lies remains relatively stable, so does the LW speed. Shortly, the good linear relationship  
341 reveals that the variation of temperature during PTL (nighttime land temperature) could generally  
342 represent the variation of TDLS during PTL while the daytime land temperature variation could not  
343 represent the TDLS variation during PTS. In our previous study, we also found through observation that  
344 the daily lowest temperature (DLT) was well negatively related to LW speed while the SW speed was  
345 more related to *in situ* downwelling solar radiation rather than merely land temperature (Shen et al.,  
346 2021), which was similar to the findings here. It could be inferred that although the land temperature  
347 during daytime increased during mega fire events, TDLS was still narrowed during fire events. If we  
348 only consider the land temperature, the SW speed should have increased during fire events because SW

349 circulation is formed due to warmer land and colder sea. Consequently, there should be other factors  
350 which could cause decreased TDLS during PTS, which is the direct cause of decreased SW speed  
351 decrease. We would investigate this in the following sections.

### 352 **3.3 The distribution and FRP of fire spots**

353 Since the heating effect depends largely on the distance between the area heated and the heat center, it is  
354 necessary to examine the distribution of fire spots in January over the years, which is shown in Figure 6.

355 It can be seen that fire spots scattered all over the eastern part of Australia in January over the years  
356 during January. January is the middle of Australian summer which is the season when wild fires  
357 happenare the most frequently (Yang et al., 2021). Apart from 2020, other years also witnessed

358 considerable scattered fire spots all over the coastal and inland regions. It is obvious that there was an  
359 extreme fire center in the southeastern corner of Australia with great density of fire spots in January of  
360 2020. This was exactly the region where the 2019 Australia mega fires mainly happened. To be specific,

361 it was the eastern corner of Victoria State and the southeastern corner of New South Wales State, which  
362 conformed to many reports from media. There was also a great fire center in the southeastern corner in  
363 2003 although the scale was smaller than that in 2020. Considering the distribution of fire spots near the

364 site, the density of fire spots nearby was not higher than in other years. Instead, there seems to be more  
365 fire spots nearby the site in 2003, 2005, 2006, 2010 and 2013 in the figure. If we restrained the nearby  
366 region to areas ofwith smaller scales, year 2003 and 2013 rather than 2020 had the most nearby fire spots.

367 There exists another possibility that although the fire spots nearby the site were not more concentrated  
368 with great density in 2020 than in other years, the FRP of fire spots in 2020 was higher. This means that  
369 the fire was greater regardless of the ordinary density of spots, which could also result in more fire-

370 induced aerosol emissions. So we further examined the FRP of fire spots in 2020 and those in other years.  
371 In order to make it comparable and verifiable, the time period of data chosen here was the same as that  
372 in Figure 6. As shown in Figure 7a, both the nearby and local fire spots in 2020 were mostly within the

373 lowest FRP range, which was less than 235 MW. There were some sparse fire spots with greater FRP  
374 (235-863 MW) scattered all over the eastern part of Australia. The FRP of the fire center was higher than  
375 the FRP of other fire spots where there were many fire spots with greater FRP which belonged to the

376 range of '235-863 MW' or '863-2194 MW'. Figure 7b shows the FRP of all fire spots from 2002-2019.  
377 The FRP of nearby or local fire spots were also with the lowest values. AsWith the number of years

378 ~~number~~ increased, the density of fire spots with higher FRP (235-863 MW) increased significantly, most  
379 of which were located at inland areas of Australia continent. This indicates that scattered wild fires with  
380 low or medium FRP are common in Australia but concentrated mega fires are not so common. There  
381 were also some fire spots which belonged to the range of '235-863 MW' or '863-2194 MW' in 2003, yet  
382 the number was less and the distribution areas were smaller. Based on Figure 7, one important point we  
383 found is that there was no discrepancy between FRP of nearby or local fire spots in 2020 and that of  
384 nearby or local fire spots in other years. So the possibility mentioned above was discarded.

385 Based on the analysis above, the nearby fire spot density and FRP in 2020 were both at the same level as  
386 in other years for local regions near the site. This implies that the heating effect of nearby fire spots did  
387 exist in 2020, contributing to the increase of land temperature to some extent (especially nighttime land  
388 temperature), but it was not likely the major cause of land temperature anomaly. Fluctuation in land  
389 temperature might be caused by combined mechanisms including some other potential factors. In other  
390 words, the heating effect of fire spots does not necessarily correspond to the observed air temperature  
391 increase. For example, Figure 4b and c show that there were negative land temperature anomalies in  
392 2003 but actually this year witnessed greater density of nearby or local fire spots. In real situation, the  
393 scale of SLB is quite small. The fire spots might be quite a long distance away from the area where  
394 vertical stream of SLB lies as a result of which the heating effect is weak.

### 395 **3.4 The spatial distribution of aerosols**

396 Large fires would have great aerosol emissions which would affect the *in situ* solar radiation and  
397 then the radiation budget. Based on the basic physical mechanism of SLB formation, the observed  
398 decreased SW and LW speeds demonstrated the decreased TDLS. As mentioned above, the heating effect  
399 of nearby fire spots was weak and did not become more significant in 2020. So the more important factors  
400 bringing about the decrease of SW and LW speeds should be closely related to TDLS rather than the land  
401 temperature only. The TDLS during SLB formation is highly related to the *in situ* downwelling solar  
402 radiation. As the shortwave radiation increases, the TDLS becomes larger due to the different heat  
403 capacities between land and sea. SW forms and prevails when TDLS is enough to drive thise  
404 thermodynamic circulation. During nighttime, the land-sea system is the heater for upper atmosphere as  
405 they both gives out heat and undergoes energy loss in the form of longwave radiation. As the outgoing  
406 longwave radiation increases, the TDLS also becomes larger due to the different heat capacities

407 ~~between~~ of land and sea. Then the LW forms in the similar way as SW forms.

408 Based on discussions above, *in situ* downwelling solar radiation is a crucial influencing factor ~~offer~~ SW

409 speed. Considering that aerosol is an important factor affecting *in situ* downwelling solar radiation, it is

410 necessary for us to check the temporal and spatial variations of aerosols over the years. Figure 8 and

411 Figure 9 shows the spatial distribution of AOD of total aerosols (TA-AOD) over the years using MERRA-

412 2 and MODIS aerosol product, respectively. It shows that except for a little overestimation of AOD in

413 the fire center in 2020, the overall distribution and value of AOD revealed by MERRA-2 agreed well

414 with those revealed by MODIS. Both MERRA-2 and MODIS shows that there was a burst of aerosols in

415 fire center during January in 2003 and 2020 and the latter was much more severe. Especially for the site

416 learned in this study, the difference of AODs between MERRA-2 (approximately 0.26) and MODIS

417 (approximately 0.29) was very small. Thus, MERRA-2 agreed well with both MODIS and AERONET

418 in terms of AOD during mega fires and it has higher spatial resolution than MODIS. Considering all

419 these aspects and the focus of the study, we used MEERA-2 product in the analysis on local aerosol

420 variations in the following sections. Figure 8 shows that ~~Over the years,~~ the background level of TA-

421 AOD was generally low in Australia over the years, implying that Australia was less polluted from human

422 ~~activities~~ pollution. The TA-AOD in 2020 increased significantly compared with the average level. It can

423 be seen that there was a maximum value center in the southeast corner, which overlapped the region of

424 fire spots center (Figure 6). The peripheral area of maximum value center was covered with isopleth

425 showing the characteristics of free diffusion of aerosols in the air. There was also a maximum value

426 center in 2003 whose scale was smaller, overlapping the smaller region of fire center in 2003. Based on

427 findings from these three aspects, it can be concluded that the mega fire center was the main source of

428 large amounts of aerosols ~~amounts~~ around the site location. In general, the TA-AOD was about 240% of

429 the multi-years' average level at the site, while the TA-AOD in the fire center was at a more astonishing

430 level, accounting for more than 420% of ~~that at the local site of Brisbane~~ multi-years' average level at

431 ~~the site~~. Aerosol could significantly affect the *in situ* downwelling solar radiation through direct radiative

432 forcing. Turnock et al. (2015) calculated the relationship between AOD and surface solar radiation (SSR)

433 and found that when the background value is low over the years, the SSR increases by 10% as AOD

434 varies from 0.32 to 0.16. In this study, the TA-AOD increased even more significantly (240%)

435 considering the low background value. Normally, when we talk about the radiative forcing of aerosols in

436 the form of SSR difference, it means the instantaneous radiative forcing. However, the formation of SLB

437 is the result of different levels of radiation accumulations between land and sea. So the effect of aerosols  
438 on the total *in situ* downwelling solar radiation can further accumulate in the process of SLB formation  
439 and results in even more significant impacts on the change of surface temperature.

440 Apart from aerosols, clouds could play an even more important role in the radiation budget. The COD  
441 and cloud fraction anomaly at this site are shown in Figure 109. The time range was from 2003 to 2020  
442 due to data availability. It can be seen that both the cloud fraction and COD in 2003 were at an obvious  
443 low level, while both the cloud fraction and COD in 2020 showed a tiny negative anomaly. Based on the  
444 spatial distribution of TA-AOD, both 2003 and 2020 witnessed a soar in TA-AOD at the site while TA-  
445 AOD increased more significantly in 2020. Figure 3 shows that there was a slump in SLB number in  
446 2020 while not in 2003, while Figure 4 shows that there were positive anomalies of both SW and LW  
447 speeds in 2003. Many previous studies on SLB have pointed out that high level of *in situ* downwelling  
448 solar radiation is favorable for SLB formation and SLB speed increase (Shen and Zhao, 2020; Shen et  
449 al., 2021, Miller et al., 2013). Our previous study in monsoon climate region also showed that there was  
450 a positive linear relationship between *in situ* downwelling solar radiation and SW speed (Shen and Zhao,  
451 2020). As known, the *in situ* downwelling solar radiation is determined by both cloud and aerosols  
452 through their combined ‘Umbrella Effect’. The finding shown in Figures 3 and 4 could be explained by  
453 the radiative cooling effects of aerosols and clouds. Although there was positive anomaly of TA-AOD in  
454 2003, the COD and cloud fraction was less than the average, offsetting the aerosols’ negative radiative  
455 forcing effect. *In situ* downwelling solar radiation of the regional sea-land system was still ensured so  
456 that the SLB happened with a normal frequency (Figure 3) and with an even larger speed (Figure 4). The  
457 *in situ* downwelling solar radiation in January of 2020 should be lower than the average, considering the  
458 tiny negative anomaly in both COD and cloud fraction and the significant increase in TA-AOD. The  
459 increased radiative forcing effect of TA-AOD was accumulated during the formation of SW. In  
460 conclusion, during daytime, the negative radiative forcing effect of total aerosols was the determinant  
461 factor to weaken the *in situ* downwelling solar radiation, resulting in lower level of TDLS and then  
462 decreased SW speed.

463 Mega fire events are special in emitting large amounts of carbonaceous aerosols which include OC and  
464 BC. The OC is a very good scatter to solar radiation. Thus, among all the aerosols, OC could be an  
465 important contributor to the weakened TDLS during SW formation. Figure 110 shows the spatial  
466 distribution of OC over the years. The spatial distribution of OC was also similar as the fire spot

467 distribution, which further confirmed that the source of great aerosol emissions was ~~the from~~ mega fire  
468 ~~centerevents~~. There were extreme value centers in the fire center in both 2003 and 2020. Same as ~~what~~  
469 ~~we~~ found earlier, it can be seen that the large value spread to farther place in 2020 than 2003, indicating  
470 that the fire events were more severe in 2020 than ~~in~~ 2003. Similarly, the background value of OC at the  
471 site was low on average. The specific value of OC-AOD at Brisbane site in 2020 was about 630% of the  
472 multi-years' average, which was even higher than that of total aerosol. This is easy to understand because  
473 the fire center is also covered with plants and trees and the combustion of them can bring significant  
474 amounts of carbonaceous aerosols. Zhang et al. (2017) estimated the radiative forcing of OC globally  
475 using BCC\_AGCM2.0\_CUACE/Aero model, which showed that Brisbane was within the large value  
476 area with high levels of negative radiative forcing at the top of atmosphere. They also owed this to  
477 biomass combustion. Thus, both total aerosol and OC made great contributions to SW speed decrease by  
478 decreasing *in situ* downwelling solar radiation in January ~~of~~ 2020.

479 The result above is analyzed based on the impacts of aerosols on solar radiation. However there is almost  
480 no shortwave radiation during nighttime. Then one question pops up: why was the slump of LW speed  
481 more significant?; ~~This-which~~ indicated that the TDLS was significantly weakened at night in January ~~of~~  
482 2020? While the heating effect of fire spots on nighttime land temperature did exist which was more  
483 significant than that during daytime, it was not likely the main cause of weakened TDLS based on FRP  
484 and fire spot distribution analysis. We next ~~investigatedechecked~~ the spatial distribution of BC over the  
485 years in Figure 12. It shows that BC-AOD at the site was about 425% of the multi-years' average level  
486 with the extreme value center overlapping the area of that of fire spots density. Similar as the distribution  
487 of TA-AOD and OC-AOD, the peripheral areas of maximum value center are covered with isopleth  
488 showing the characteristics of free diffusion. BC is well known as a kind of absorbing aerosols which is  
489 reported to have wider range of absorbing band than greenhouse gases, which can absorb broadband  
490 radiation from visible light to infrared wavelength (Zhang et al., 2017). During daytime, it can absorb  
491 solar radiation, longwave radiation from the warmer land, and shortwave radiation from local fires.  
492 During nighttime, it has a warming effect on both atmosphere and Earth surface through longwave  
493 radiation. As a result, it has a warming effect on the Earth-atmosphere system including the surface of  
494 the regional land-sea system so that there was a temperature soar shown in Figure 4b. The soaring BC  
495 during the mega fire heated the local atmosphere, which was like adding a 'heater' in the air. The 'heater'  
496 then gave out downward longwave radiation to the regional land-sea system. Just like the sun during

497 daytime, this could trigger a SW circulation anomaly, weakening LW circulation. Considering the BC  
498 burst during mega fire ~~ese events~~, it is nothing weird about its dominant role in local land temperature  
499 increase during nighttime. The mechanism proposed above can be summarized as follows. During  
500 nighttime, the formation of LW originates from the process of heat release ~~from~~ both land and sea. As  
501 they both lose heat with different paces due to different heat capacities, the TDLS is enlarged. During  
502 the mega fire ~~s-event~~, the upper atmosphere of the regional land-sea system is heated so that the vertical  
503 temperature gradient is weakened, which is unfavorable for heat release ~~from~~ both sea and land  
504 surfaces. As a result, the TDLS is significantly weakened.

505 Another potential contributing accelerator is CO<sub>2</sub> which is also the product of fires due to the combustion  
506 of plants and trees. CO<sub>2</sub> is a kind of greenhouse gas which is likely to be engaged in the same mechanism  
507 as BC to reduce TDLS during nighttime except that CO<sub>2</sub> cannot affect the downwelling solar radiation.  
508 Details about this is not repeated again. However we should note that the effect of CO<sub>2</sub> is based on  
509 theoretical analysis rather than observational verification due to the lack of accurate observation data.  
510 Both BC and CO<sub>2</sub>'s warming effects ~~-increase~~ reduce TDLS during daytime, which partially offset the  
511 ~~enhanced strong negative~~ radiative forcing effect of total aerosols, but their combined warming effect is  
512 more significant during nighttime than during daytime. That is most likely the reason (at least partially)  
513 that SW speed had negative anomaly but was less significant than LW speed.

514 What we discussed above are all factors whose influences were restrained to a small scale. Although SLB  
515 is a small scale system, it can still be affected by the variations of signals in a large scale, since the local  
516 temperature is affected by both regional forcing and the variation of large scale background temperature  
517 field. In our previous study, we weighed their contributions qualitatively (Shen et al., 2019). In this study,  
518 ~~w~~We here simply discuss the potential effect of the change in large scale SST. Hirsch and Koren (2021)  
519 emphasized~~warned~~ the effect of record-breaking aerosol emission from this mega fire on cooling the  
520 oceanic areas. On a large scale, its average radiative forcing on sea surface was  $-1.0 \pm 0.6 \text{ W/m}^2$ . The  
521 temperature decrease of large scale sea surface could have negative forcing on the SST at a regional scale,  
522 though the specific temperature variation of the sea surface where the SLB vertical stream lies might not  
523 be the same.

524 We summarized all the influencing factors of TDLS at both regional and large scales in Table 2. Among  
525 all these factors, aerosols, BC, OC and CO<sub>2</sub> had direct forcing on TDLS by changing the solar radiation  
526 reaching the regional sea-land system. In contrast, heating effect of fire spots and large scale SST signal

527 had forcing on land temperature and regional SST respectively thus further had different forcing effects  
528 on TDLS during daytime and nighttime. During 2019 Australia mega fires, TDLS during daytime and  
529 nighttime both decreased under their combined forcing effects, which could be inferred from the  
530 anomalies of SLB speed. Clearly, the directions of all forcing effects ~~offrom~~ different factors were the  
531 same during nighttime. That was why LW speed decreased much more significantly than SW speed did.  
532 The negative radiative forcing effect of total aerosols was the determinant cause for TDLS decrease  
533 during daytime, which could only be partially offset by other factors.

### 534 3.5 Source of aerosols

#### 535 3.5.1 Fire center's emission

536 As indicated earlier, year 2020 did not have advantages over other years in terms of local and nearby fire  
537 spot density and FRP induring January. Note that certain land cover type could also increase the aerosol  
538 emissions. For example, if there were more combustible such as forests or plants, the fires could emit  
539 more carbonaceous aerosols in form of smoke. Considering this possibility, we further checked the latest  
540 version of land cover in Australia online (<http://maps.elie.ucl.ac.be/CCI/viewer/index.php>). It was  
541 updated to 2019 which overlapped with the starting time of 2019 Australia mega fires s-events. It showed  
542 that the areas and density of flora near the site were stable over the years, implying that the soar in local  
543 aerosols during mega fires s-events was not likely caused by the change of land cover either.

544 As Figures ~~6, 8, 8 and 11 and 12~~ show, the distributions of fire spots, TA-AOD, BC-AOD and OC-AOD  
545 were quite similar as each other. In the fire center, both the density and FRP of fire spots were much  
546 higher in January of 2020 than in January of other years, ~~which~~ These are all based on distribution  
547 characteristics at a large scale. In order to show the fire situation at the fire center more accurately, we  
548 magnified the FRP map to restrain the areas to merely the fire center, which is shown in Figure ~~13~~ 32. As  
549 shown, the fire spot density was quite high in this region ~~area~~, especially along coastal areas. Compared  
550 with other areas, the fire center had much more fire spots with higher FRP. The spots with FRP from 235  
551 to 864 MW were evenly distributed in all fire ~~fire~~ areas, surrounded by low FRP spots with high density.  
552 There were quite a few spots with even higher FRP ranging from 864 to 2,194 MW, which could not be  
553 found in other periphery areas (Figure 7a). In some areas at the fire center, we could even find fire spots  
554 with FRP ranging from 2,194 to 5,232 MW. All these distribution characteristics of fire spots suggested  
555 the possibility of large amounts of aerosols including smoke being emitted into the atmosphere, after

556 which a great concentration gradient in the horizontal direction formed between the fire center and farther  
557 areas. Based on the basic Chemistry law, irreversible free diffusion would happen in this process. As the  
558 concentration gap increases, the diffusion efficiency also increases. The distribution of contour lines in  
559 Figures 8, ~~110~~ and ~~121~~ also shows the characteristics of free diffusion. Similar mechanism works out for  
560 the spatial distribution of CO<sub>2</sub> during the fire events.

### 561 3.5.2 Analysis on the background wind field

562 Apart from free diffusion, wind is crucial for pollution transport including aerosols (Walcek, 2002). Also,  
563 wind is a key factor ~~of influencing~~ the near-surface CO<sub>2</sub> distribution (Cao et al., 2017). Zhang et al. (2017)  
564 confirmed that BC could be transported ~~overthrough a~~ long distances in mid-latitude areas. The transport  
565 distance of OC was even longer than that of BC. It is necessary for us to look into the background wind  
566 field in order to know the likely aerosol transport from the fire center to the site. Yang et al. (2021)  
567 retrieved the average status of the vertical distribution of various aerosols in southeastern Australia during  
568 2019 Australia mega fires and found most of them accumulated under 3 km, which is about 700 hPa.  
569 Figure ~~143~~ shows the monthly average of background wind field based on wind information at pressure  
570 levels from 1000 hPa to 700 hPa ~~induring~~ January ~~ofn~~ 2020. The red cross symbols represent the fire  
571 spot in this figure. The average background wind field clearly revealed the existence of southern  
572 hemisphere's westerlies and subtropical high. The fire center was approximately located at the  
573 intersection of the northern boundary of westerlies and southwestern boundary of subtropical high. Since  
574 January is the middle month of Australian summer, the subtropical high developed quite vigorously, some  
575 of which stretched into the eastern part of Australian continent. It covered the areas where most fire spots  
576 were located. At a large scale, this brought quite hot and dry background meteorological field, which was  
577 favorable for the development and persistence of wild fires. Based on the average status of wind fields  
578 at different pressure levels, the subtropical high and westerlies together formed a background wind field  
579 blowing from the site to fire center, which was ~~not un~~favorable for the aerosol transport from the fire  
580 center to the site. However, we should notice that this figure merely describes the monthly average status  
581 but ignores the status of wind flows at a more accurate fine time scale. In other words, it is still possible  
582 that aerosols from the fire center were transported to the site within some short periods in January ~~of~~  
583 2020, ~~thus made contributing to~~ the significant positive aerosol anomalies in AODs shown in  
584 Figures 8, ~~9~~, ~~110~~ and ~~121~~. Based on the specific dates of SLB day during mega fires identified in previous

585 section, which were 4th, 14th, 20th and 28th in January respectively, we divided the January ~~off~~ 2020  
586 into five short time periods by excluding the identified SLB days. These five short time periods were all  
587 named as ‘No-SLB period’. We did the backward trajectory analysis during each No-SLB period to see  
588 if the aerosols from the fire center were transported to the site with the help of background wind field,  
589 thus further made this period a ‘No-SLB period’ through all the mechanisms mentioned above. It is easy  
590 to understand that the near surface concentration of aerosol should be at a high level in general not only  
591 because it was near the fire spots but also because it ~~was~~ within the boundary layer. Considering these  
592 aspects, the backward trajectory analysis was carried out at 500 m over the site. Figures 154a-e show the  
593 wind backward trajectories at this site during the five No-SLB periods respectively. During the No-SLB  
594 periods of a, c, d and e, the winds mainly came from the southern Pacific to the east of Australia continent,  
595 which could not transport aerosols from the fire center. There were winds coming from the fire center  
596 merely during period b. The northern edge of wind flow beam was quite near the fire center, then it went  
597 further towards the northeastern direction in the southern Pacific. When it reached the general position  
598 of subtropical high, it turned back to the direction of northwest before finally reaching the site. The high  
599 pressure gradient between the center and edge of the subtropical high was opposite to its moving direction,  
600 which might be the cause of its abrupt turning. Although the southwestern edge of the subtropical high  
601 itself had wind flows whose directions were away from the Australia continent at a monthly average  
602 (Figure 143), the wind flows from northern edge of southern hemisphere’s westerlies could still move  
603 along its southwestern edge as soon as they intersected with each other if smaller time scale and single  
604 level were considered (Figure 154b). Figure 154f showed the contributions of main backward trajectories  
605 based on the whole month’s statistics. The main backward trajectories were calculated after the clustering  
606 of all trajectories, whose number was based on certain mathematical method like the calculation of total  
607 spatial variation (TSV). More details of this clustering method and contribution calculation can be found  
608 on the official website of this software ([http://meteothink.org/docs/trajstat/cluster\\_cal.html](http://meteothink.org/docs/trajstat/cluster_cal.html)). It can be  
609 seen that the wind flows which could potentially bring aerosols from the fire center still had a little  
610 contribution, which accounted for 9.32% (2.87%+6.45%). In contrast, winds coming from the Pacific to  
611 the east and northeast of the Australia continent dominated the wind field at the site, whose contributions  
612 were 25.09% and 54.12% respectively. Thus, the ~~aerosol~~ contribution ~~off~~ from wind transport to increasing  
613 local aerosols should be limited, which was only found during one ~~time~~ period with time length less than  
614 10 days in January of 2020. From the perspective of multi-layers of atmosphere (0-3 km), the multi-

615 layers of background wind fields as a whole did not contribute to the aerosol and CO<sub>2</sub> transport from the  
616 fire center to the site. Therefore, the soar of aerosols including BC and OC at the site should be mainly  
617 caused by the combined effect of combustion in the fire center and great free diffusion caused by  
618 significant concentration gradient, with likely relatively weak contribution of the wind transport.

619 Most aerosols are generally within atmospheric boundary layer under normal conditions while it might  
620 be different under the situation during mega fires s-events considering the boost of vertical movement due  
621 to great heat release from fires and astonishing amounts of aerosol emissionsloadings. Smoke, as a kind  
622 of unique aerosol emissionloading with great amounts during fire events, could be essential to SW and  
623 LW speed anomalies ies due to its absorptive radiative properties, making it particularly valuable to  
624 examine its transport individually. Yang et al. (2021) analyzed the vertical distribution of smoke on  
625 southeastern parts of Australia, which included the fire center and the site, and found that the smoke  
626 accumulated at 3 km generally. Considering this aspect, we also did the backward trajectory analysis at  
627 3 km whose time division was the same as that at 500 m. The results are shown in Figure 165. As shown,  
628 the wind flow scattered more evenly at 3 km than at 500 m. There were more wind flows coming from  
629 the southwestern direction of the site. This is probably due to the fact that the magnitude and stretching  
630 area of westerlies are larger at upper atmosphere than at layers closer to the surface. During period a, b  
631 and e, there were clusters of wind flows coming from the fire center or near the fire center, which could  
632 bring aerosols to the site. Specifically, there were wind flows penetrating the fire center directly during  
633 period a and e, while the wind flows during period b are only adjacent to the north edge of fire center.  
634 Since the period b was the longest among all No-SLB periods, it did not necessarily mean that the wind's  
635 aerosol transport effect during this period was less than those during other periods although the wind  
636 flows were not directly from the fire center. The moving paths of them were similar as thoseat of wind  
637 flows in Figure 154b, which all had an abrupt turning on the Pacific to the southeast of the site. This is  
638 probably because that the south hemisphere's subtropical high developed to be quite strong during the  
639 middle of summer, making the pressure gradient exist both at 500 m and 3 km (Figure 14). Figure 165f  
640 shows the contribution of wind flows on monthly average, whose clustering number was also four. There  
641 were four main directions of wind flows, whose contribution were 28.67%, 21.86%, 11.47% and 37.99%  
642 respectively. In order to make it clear, we define these four main wind flows as wind flow clusters. The  
643 wind flow clusters with contributions of 21.86% and 11.47% were generally adjacent to the north edge  
644 of the fire center, which contained contribution of wind flows from the fire center. Due to the clustering

645 limitation of Meteoinfo, we could not extract the specific contributions of wind flows blowing directly  
646 from fire center from the total contributions of wind flow clusters (21.86% and 11.47%). But based on  
647 analysis on shorter time periods, their contributions were larger than those at 500 m because there were  
648 more No-SLB periods with wind flows blowing from fire center.

### 649 **3. Summary and discussion**

650 ~~This~~In this study, the SLB day number, SLB speed, daytime temperature and nighttime temperature at  
651 Brisbane Archerfield ~~in~~during January were calculated from 2001 to 2020 using observation data from  
652 automatic meteorological station. We have taken three steps in total to exclude the interference of winds  
653 from synoptic-scale systems in order to extract the real SLB signals. First, we used SRWF method to  
654 verify the OE-SLB and then extracted the SLB signal from original observation. Second, we defined  
655 SLB day when the whole SLB circulation is most significant and integrated. Finally, we used SLB signals  
656 during PTS (PTL) on SLB days to calculate the monthly average of SW (LW) speed. ~~In~~During the  
657 corresponding month over the years, regional cloud fraction, COD, fire spot and FRP distribution in  
658 Australia were revealed using MODIS product. [Comparison with MODIS and site observations](#)  
659 [confirmed the good quality of MERRA-2 product to reveal the variation of aerosols during mega fires.](#)  
660 ~~Consequently~~~~So~~. aerosols' ~~a~~Aerosol distributions in eastern Australia were revealed in the form of AOD  
661 using MERRA-2 product, including that of total aerosols, OC and BC. Furthermore, the background  
662 wind field and backwards wind trajectory were analyzed by ERA5 product and HYSPLIT respectively.  
663 The main findings of this study are as follows.

664 1). There was a significant slump in SLB day number (33.3% of the average level) and LW speed  
665 (decreased by 22.3% of the average level) at the site. While SW speed also decreased by 14.8% of the  
666 average level, it was not significant.

667 2). There was a burst of aerosols at the site, with TA-AOD, BC-AOD and OC-AOD ~~being~~ approximately  
668 240%, 425%, 630% of the multi-years' averages. TDLS is the direct cause of SLB while other factors  
669 influence SLB through their effects on TDLS. The variation of nighttime land temperature could  
670 generally represent the variation of TDLS during nighttime while TDLS during daytime could not be  
671 simply represented by daytime land temperature. Specifically, the significant aerosol burst was mainly  
672 responsible for the decrease of SW speed. The burst of BC at the site as well as the large-scale SST

673 decrease during mega fires were mainly responsible for the slump of LW speed. CO<sub>2</sub> emitted by nearby  
674 fire spots or transmitted from the fire center was a potential and weak factor ~~offer~~ the slump of LW speed.  
675 While the heating effect of nearby fires on TDLS was weak during both daytime and nighttime.

676 3). Emissions from fire center were mainly responsible for the local positive aerosol anomaly during  
677 mega fires ~~events~~. On average, the background wind fields from near surface to 3 km were ~~not~~  
678 ~~un~~favorable for aerosol and CO<sub>2</sub> transport. But there were likely aerosol and CO<sub>2</sub> transports through large  
679 scale wind field at single levels during shorter periods within January of 2020. Specifically, the wind  
680 flow transport at 3 km was stronger than that at 500 m, which was particularly important for smoke  
681 transport since the smoke from fires gathered at the same level. In general, free diffusion due to large  
682 concentration gradient was mainly responsible for aerosol transport and the potential CO<sub>2</sub> transport while  
683 the effect of background wind field played a second role.

684 In order to make it clear and concise to the influencing factors of SLB, we summarized their potential  
685 mechanisms in local sea-land system (Figure 176). During daytime, negative anomaly of SW speed was  
686 found at the site ~~induring~~ January ~~of~~ 2020 when Australia mega fires were most intensive. The local  
687 cloud fraction and COD were almost on an average level while there were much more aerosols during  
688 mega fires ~~events~~, which mainly came from fire center by free diffusion. They significantly weakened  
689 the *in situ* downwelling solar radiation thus further narrowed the TDLS, which was the direct cause of  
690 SW speed decrease. BC and CO<sub>2</sub> heated the atmosphere and warmed the earth-atmosphere system by  
691 longwave radiation from the heated atmosphere. Warming effect of BC and CO<sub>2</sub>, the decrease of SST at  
692 a large scale and the weak heating effect of nearby fire spots partially offset the effect of aerosols on  
693 narrowing TDLS, making the negative SW speed anomaly not exceed the multi-years' oscillation range.  
694 During nighttime, the heating effect of nearby fire spots was still weak but more significant than that  
695 during daytime. The warming effect of BC and CO<sub>2</sub> was like adding a heater in the atmosphere, which  
696 triggered a SW circulation anomaly thus resulted in a slump in LW speed. The decrease of SST at a large  
697 scale further boosted the decrease of LW speed. The slumps in both SLB speed and SLB day number  
698 could help to accumulate the local aerosols (Shen and Zhao, 2020), which further catalyzed the physical  
699 processes mentioned in the mechanism and finally formed a positive feedback mechanism under a  
700 scenario of mega fires.

701 Essentially, narrowed TDLS was the direct cause of SLB speed decrease, which was affected by various  
702 factors in the form of either shortwave radiation or longwave radiation. It not only weakened the SLB

703 speed, but also brought about a slump in SLB day number. The *in situ* radiation, including both longwave  
704 and shortwave radiation reaching the ground, has a direct impact on the TDLS considering the basic  
705 physical mechanism of SLB formation. Note that the specific weather condition, cloud fraction, COD,  
706 and the type of clouds and aerosols could all affect the *in situ* radiation. Apart from *in situ* radiation, the  
707 heat release in urban areas, heat waves, heating effect of nearby heat sources, large-scale signals of SST  
708 and land surface temperature variation could all affect TDLS by changing either the local land  
709 temperature or SST. The large-scale signals of temperature variations could be caused by either natural  
710 variability or human variability. Normally, SLB forms when the TDLS is obvious and the background  
711 wind field is mild. So the condition of large scale wind field such as monsoon is also an important  
712 influencing factor of SLB. Apart from the slump in both SLB day number and LW speed during mega  
713 fire events, there were smaller fluctuations in both of their trends, which is need further study in future.

714 **Data availability.** The Dynamic Land Cover Dataset (DLCD) can be approached through Geoscience  
715 Australia (<http://www.ga.gov.au/scientific-topics/earth-obs/accessing-satellite-imagery/landcover>,  
716 Lyburner et al., 2015). MERRA-2 Reanalysis data can be approached through the NASA Global  
717 Modeling and Assimilation Office (<https://gmao.gsfc.nasa.gov/reanalysis/MERRA-2/>, GlobalModeling  
718 and Assimilation Office (GMAO), 2015). MODIS observation data can be approached through Earthdata  
719 center managed by NOAA (<https://earthdata.nasa.gov/search?q=MCD06>). GDAS data used in HYSPLIT  
720 data are accessible through the NOAA READY website (<http://www.ready.noaa.gov>, NOAA, 2016). Fire  
721 spot and FRP data can be approached from MODIS MCD14 product managed by NOAA  
722 (<https://earthdata.nasa.gov/search?q=MCD14>). The wind and temperature observation data from NOAA  
723 global observation network can be approached by NOAA's official website  
724 (<http://www1.ncdc.noaa.gov/pub/data/noaa/>). The ERA5 data can be approached through official  
725 website of Copernicus project (<https://climate.copernicus.eu/climate-reanalysis>).

726 **Author contributions.** CFZ and LXS developed the ideas and designed the study. LXS, XCY, YKY and  
727 PZ contributed to collection and analyses of data. LXS and XCY performed the analysis and prepared  
728 the manuscript. CFZ supervised and modified the manuscript. All authors made substantial contributions  
729 to this work.

730 **Competing interests.** The authors declare that they have no conflict of interest.

731 **Acknowledgements.** This work was supported by the Ministry of Science and Technology of China  
732 National Key Research and Development Program (2019YFA0606803), the National Natural Science  
733 Foundation of China (41925022), the State Key Laboratory of Earth Surface Processes and Resources  
734 Ecology, and the Fundamental Research Funds for the Central Universities.

## 735 **Reference**

736 Albrecht, B. A.: Aerosols, Cloud Microphysics, and Fractional Cloudiness, *Science*, 245, 1227–1230,  
737 <https://doi.org/10.1126/science.245.4923.1227>, 1989.

738 Cao, L. Z., Chen, X., Zhang, C., Kurban, A., Yuan, X. L., Pan, T., and Maeyer, P.: The temporal and  
739 spatial distributions of the near-surface CO<sub>2</sub> concentrations in central Asia and analysis of their  
740 controlling factors, *Atmosphere*, 8, 1-14, <http://doi.org/10.3390/atmos8050085>, 2017.

741 Charlson, R. J., Schwartz, S. E., Hales, J. M., Cess, R. D., Coakley, J. A., Hansen, J. E., and Hofmann,  
742 D. J.: Climate forcing by anthropogenic aerosols, *Science*, 255, 423–430, 1992.

743 Chuang, C. C., Penner, J. E., Prospero, J. M., Grant, K. E., Rau, G. H., and Kawamoto, K.: Cloud  
744 susceptibility and the first aerosol indirect forcing: Sensitivity to black carbon and aerosol  
745 concentrations, *J. Geophys. Res.-Atmos.*, 107, 4564, <https://doi.org/10.1029/2000JD000215>, 2002.

746 Cuxart, J., Jiménez, M.A., Prtenjak, M.T., and Grisogono, B.: Study of a sea-breeze case through  
747 momentum, temperature, and turbulence budgets, *J. Appl. Meteorol. Climatol.*, 53, 2589–2609,  
748 2014.

749 Garrett, T. J. and Zhao, C.: Increased Arctic cloud longwave emissivity associated with pollution from  
750 mid-latitudes, *Nature*, 440, 787–789, <https://doi.org/10.1038/nature04636>, 2006.

751 Giglio, L., Schroeder, W., and Justice, C. O.: The collection 6 MODIS active fire detection algorithm and  
752 fire products, *Remote Sens. Environ.*, 178, 31–41, <https://doi.org/10.1016/j.rse.2016.02.054>, 2016.

753 Grandey, B. S., Lee, H. H., and Wang, C.: Radiative effects of interannually varying vs. interannually  
754 invariant aerosol emissions from fires, *Atmos. Chem. Phys.*, 16, 14495–14513,  
755 <https://doi.org/10.5194/acp-16-14495-2016>, 2016.

756 Han, W. C., Li, Z. Q., Wu, F., Zhang, Y., and Lee, S. S.: Opposite effects of aerosols on daytime urban

757 heat island intensity between summer and winter, *Atmos. Chem. Phys.*, 20, 6479–6493,  
758 <https://doi.org/10.5194/acp-2020-162>, 2020.

759 Hirsch, E., and Koren, I.: Record-breaking aerosol levels explained by smoke injection into the  
760 stratosphere, *Science*, 371, 1269-1274, <http://doi.org/10.1126/science.abe1415>, 2021.

761 Intergovernmental Panel on Climate Change, *Climate Change 2013: The Physical Science Basis.*  
762 Contribution of Working Group I to the Fifth Assessment Report of the Intergovernmental Panel on  
763 Climate Change, 1535 pp, Cambridge Univ. Press, Cambridge, U. K., and New York, 2013.

764 Jacobson, M. Z. : Strong radiative heating due to the  $\gamma$ -mixing state of black carbon in  $\gamma$ -atmospheric  
765 aerosols, *Nature*, 409, 695-697, 2001.

766 Jacobson, M. Z.: Effects of biomass burning on climate, accounting for heat and moisture fluxes, black  
767 and brown carbon, and cloud absorption effects, *J. Geophys. Res.-Atmos.*, 119, 8980–9002,  
768 <https://doi.org/10.1002/2014jd021861>, 2014.

769 Jia, S. Q., Jing, J. L., Ju, E. D., and Chi, W. B.: Discussions on the temperature and pressure fields in a  
770 mega forest fire zone, *J. Nort. Fore. Uni.*, 15, 226-232,  
771 <http://doi.org/10.13759/j.cnki.dlxb.1987.s4.028>, 1987.

772 Kloss, C., Berthet, G., Sellitto, P., Ploeger, F., Bucci, S., Khaykin, S., Jégou, F., Taha, G., Thomason, L.  
773 W., Barret, B., Flochmoen, E., Hobe, M., Bossolasco, A., Bègue, N., and Legras, B.: Transport of  
774 the 2017 Canadian wildfire plume to the tropics via the Asian monsoon circulation, *Atmos. Chem.*  
775 *Phys.*, 19, 13547–13567, <https://doi.org/10.5194/acp-19-13547-2019>, 2019.

776 Kusaka, H., Kimura, F., Hirakuchi, H., and Mizutori, M.: The effects of land-use alteration on the sea  
777 breeze and daytime heat island in the Tokyo metropolitan area, *J. Meteorol. Soc. Jpn.*, 78, 405–420,  
778 [https://doi.org/10.2151/jmsj1965.78.4\\_405](https://doi.org/10.2151/jmsj1965.78.4_405), 2000.

779 Li, J. W., Yang, L. Q., Li, X. W., and Zheng, H. R.: Visualization of local wind field based forest-fire's  
780 forecast modeling for transportation planning, *Multimed. Tools. Appl.*, 1, 1-15,  
781 <http://doi.org/10.1007/s11042-016-3357-7>, 2016.

782 Luhar, A. K., Mitchell, R. M., Meyer, C. P., Qin, Y., Campbell, S., Gras, J. L., and Parry, D.: Biomass  
783 burning emissions over northern Australia constrained by aerosol measure-  
784 ments: II—Model validation, and impacts on air quality and radiative forcing, *Atmos. Environ.*, 42, 1647–  
785 1664, <https://doi.org/10.1016/j.atmosenv.2007.12.040>, 2008.

786 Lyburner, L., Tan, P., McIntyre, A., Thankappan, M., and Sixsmith, J.: Dynamic Land Cover Dataset

787 Version 2.1. Geoscience Australia, Canberra, available at:  
788 <http://pid.geoscience.gov.au/dataset/ga/83868> (last access: 31 January 2021), 2015.

789 Ma, Y., Gao, R. Z., and Miao, S. G.: Impacts of urbanization on summer-time SLB circulation in Qingdao,  
790 *Acta. Sci. Circumst.*, 33, 1690–1696, <https://doi.org/10.13671/j.hjkxxb.2013.06.030>, 2013.

791 Mallet, M. D., Desservettaz, M. J., Miljevic, B., Milic, A., Ristovski, Z. D., Alroe, J., Cravigan, L. T.,  
792 Jayaratne, E. R., PatonWalsh, C., Griffith, D. W. T., Wilson, S. R., Kettlewell, G., vander Schoot,  
793 M. V., Selleck, P., Reisen, F., Lawson, S. J., Ward, J.,  
794 Harnwell, J., Cheng, M., Gillett, R. W., Molloy, S. B., Howard, D., Nelson, P. F., Morrison, A. L.,  
795 Edwards, G. C., Williams, A. G., Chambers, S. D., Werczynski, S., Williams, L. R., Winton, V. H.  
796 L., Atkinson, B., Wang, X., and Keywood, M. D.: Biomass burning emissions in north Australia  
797 during the early dry season: an overview of the 2014 SAFIRED campaign, *Atmos. Chem. Phys.*,  
798 17, 13681–13697, <https://doi.org/10.5194/acp-17-13681-2017>, 2017.

799 McCoy, D. T., and Hartmann, D. L.: Observations of a substantial cloud-aerosol indirect effect during the  
800 2014–2015 Bárðarbunga-Veiðivötnfissure eruption in Iceland, *Geophys. Res. Lett.*, 42, 10409–  
801 10414, <http://doi.org/10.1002/2015GL067070>, 2015.

802 Meyer, C. P., Luhar, A. K., and Mitchell, R. M.: Biomass burning emissions over northern Australia  
803 constrained by aerosol measurements: I – Modelling the distribu-  
804 tion of hourly emissions, *Atmos. Environ.*, 42, 1629–1646,  
805 <https://doi.org/10.1016/j.atmosenv.2007.10.089>, 2008.

806 Miller, S. T. K., Keim, B. D., Talbot, R. W., and Mao, H.: Sea breeze: Structure, forecasting, and impacts,  
807 *Rev. Geophys.*, 41, 1011, <http://doi:10.1029/2003RG000124>, 2013.

808 Mitchell, R. M., Forgan, B. W., Campbell, S. K., and Qin, Y.: The climatology of Australian tropical  
809 aerosol: Evidence for regional correlation, *Geophys. Res. Lett.*, 40, 2384–2389,  
810 <https://doi.org/10.1002/grl.50403>, 2013.

811 Mitchell, R. M., O’Brien, D. M., and Campbell, S. K.: Characteristics and radiative impact of the aerosol  
812 generated by the Canberra firestorm of January 2003, *J. Geophys. Res.-Atmos.*, 111, D02204,  
813 <https://doi.org/10.1029/2005jd006304>, 2006.

814 Nai, F. B., Zhao, L. N., and Wu, J. R.: Impacts of sea-land and mountain-valley circulations on the air  
815 pollution in Beijing-Tianjin-Hebei: a case study, *Environ. Pollut.*, 234, 429–438,  
816 <https://doi.org/10.1016/j.envpol.2017.11.066>, 2018.

817 Ohneiser, K., Ansmann, A., Baars, H., Seifert, P., Barja, B., Jimenez, C., Radenz, M., Teisseire, A., Floutsi,  
818 A., Haarig, M., Foth, A., Chudnovsky, A., Engelmann, R., Zamorano, F., Bühl, J., and Wandinger,  
819 U.: Smoke of extreme Australian bushfires  
820 observed in the stratosphere over Punta Arenas, Chile, in January 2020: optical thickness, lidar ratios,  
821 and depolarization ratios at 355 and 532nm, *Atmos. Chem. Phys.*, 20, 8003–8015,  
822 <https://doi.org/10.5194/acp-20-8003-2020>, 2020.

823 Portin, H., Mielonen, T., Leskinen, A., Arola, A., Pärjälä, E., Romakkaniemi, S., Laaksonen, A., Lehtinen,  
824 K. E. J., and Komppula, M.: Biomass burning aerosols observed in Eastern Finland during the  
825 Russian wildfires in summer 2010 e Part 1: In-situ aerosol characterization, *Atmos. Environ.*, 47,  
826 269-278, <http://doi:10.1016/j.atmosenv.2011.10.067>, 2012.

827 Ramana, M. V., Ramanathan, V., Feng, Y., Yoon, S. C., Kim, S. W., Carmichael, G. R., and Schauer, J.  
828 J.: Warming influenced by the ratio of black carbon to sulphate and the black-carbon source,  
829 *Nature. Geosci.*, 1, 542-545, <http://doi.org/10.1038/NGEO918>, 2010.

830 Rajib, P., and Heekwa, L.: Estimation of the effective zone of sea/land breeze in a coastal area, *Atmos.*  
831 *Pollut. Res.*, 2, 106–115, <https://doi.org/10.5094/APR.2011.013>, 2010.

832 Sarker, A., Saraswat, R. S., Chandrasekar, A.: Numerical study of the effects of urban heat island on the  
833 characteristic features of the sea breeze circulation, *J. Earth Syst. Sci.*, 107, 127–137, 1998.

834 Shen, L. X., Zhao, C. F., Ma, Z. S., Li, Z. Q., Li, J. P., and Wang, K. C.: Observed decrease of summer  
835 sea-land breeze in Shanghai from 1994 to 2014 and its association with urbanization, *Atmos. Res.*,  
836 227, 198-209, <http://doi.org/10.1016/j.atmosres.2019.05.007>, 2019.

837 Shen, L. X., and Zhao, C. F.: Dominance of Shortwave Radiative Heating in the Sea–Land Breeze  
838 Amplitude and its Impacts on Atmospheric Visibility in Tokyo, Japan, *J. Geophys. Res.-Atmos.*,  
839 125, 1-19, <https://doi.org/10.1029/2019jd031541>, 2020.

840 Shen, L. X., Zhao, C. F., and Yang, X. C.: Insight Into the Seasonal Variations of the Sea-Land Breeze in  
841 Los Angeles With Respect to the Effects of Solar Radiation and Climate Type, *J. Geophys. Res.-*  
842 *Atmos.*, 126, 1-21, <https://doi.org/10.1029/2019jd033197>, 2021.

843 Shen, L. X., Zhao, C. F., and Yang, X. C.: Climate-Driven Characteristics of Sea-Land Breezes Over  
844 the Globe, *Geophys. Res. Lett.*, 48, 1-10, <https://doi.org/10.1029/2020GL092308>, 2021.

845 Stageberg, M. S.: Sensitivities of simulated fire-induced flows to fire shape and background wind profile  
846 using a cloud-resolving model, Master Dissertation, Michigan State University, ProQuest

847         Dissertations Publishing, 10816178, 2018.

848     Torres, O., Jethva, H., Ahn, C., Jaross, G., and Loyola, D. G.: TROPOMI aerosol products: evaluation  
849         and observations of synoptic-scale carbonaceous aerosol plumes  
850     during 2018–2020, *Atmos. Meas. Tech.*, 13, 6789–6806, <https://doi.org/10.5194/amt-13-6789-2020>,  
851         2020.

852     Turnock, S. T., Spracklen, D. V., Carslaw, K. S., Mann, G. W., Woodhouse, M. T., Forster, P. M.,  
853         Haywood, J., Johnson, C. E., Dalvi, M., Bellouin, N., and Sanchez-Lorenzo, A.: Modelled and  
854         observed changes in aerosols and surface solar radiation over Europe between 1960 and 2009,  
855         *Atmos. Chem. Phys.*, 15, 9477–9500, <https://doi.org/10.5194/acp-15-9477-2015>, 2015.

856     van der Werf, G. R., Randerson, J. T., Giglio, L., Collatz, G. J., Kasibhatla, P. S., and Arellano Jr., A. F.:  
857         Interannual variability in global biomass burning emissions from 1997 to 2004, *Atmos. Chem. Phys.*,  
858         6, 3423–3441, <https://doi.org/10.5194/acp-6-3423-2006>, 2006.

859     Vermote, E., Ellicott, E., Dubovik, O., Lapyonok, T., Chin, M., Giglio, L., and Roberts, G. J.: An  
860         approach to estimate global biomass burning emissions of organic and black carbon from MODIS  
861         fire radiative power, *J. Geophys. Res.-Atmos.*, 114, D18205, <https://doi.org/10.1029/2008jd011188>,  
862         2009.

863     Walcek, C. J.: Effects of wind shear on pollution dispersion, *Atmos. Environ.*, 36, 511–517,  
864         [http://doi.org/10.1016/s1352-2310\(01\)00383-1](http://doi.org/10.1016/s1352-2310(01)00383-1), 2002.

865     Wang, Y., Jiang, J. H., and Su, H.: Atmospheric responses to the redistribution of anthropogenic aerosols,  
866         *J. Geophys. Res.-Atmos.*, 120, 9625–9641, <http://doi.org/10.1002/2015JD023665>, 2015.

867     Xue, D. Q., Zheng, Q. L., and Qian, X. Z.: Features of sea-land circulation with its influence over  
868         Shandong Peninsula, *J. Nanjing Inst. Meteorol.*, 18, 293–299,  
869         <https://doi.org/10.13878/j.cnki.dqkxxb.1995.02.021>, 1995.

870     Yan, H., and Anthes, R. A.: The effect of latitude on the sea breeze, *Mon. Wea. Rev.*, 115, 936–956, 1987.

871     Yang, X., Zhao, C. F., Zhou, L., Wang, Y., and Liu, X.: Distinct impact of different types of aerosols on  
872         surface solar radiation in China, *J. Geophys. Res. Atmos.*, 121, 6459–6471,  
873         <http://doi.org/10.1002/2016JD024938>, 2016.

874     Yang, X. C., Zhao, C. F., Yang, Y. K., Yan, X., and Fan, H.: Statistical aerosol properties associated with  
875         fire events from 2002 to 2019 and a case analysis in 2019 over Australia, *Atmos. Chem. Phys.*, 21,  
876         3833–3853, <https://doi.org/10.5194/acp-21-3833-2021>, 2021.

877 Zhang, H., Wang, Z. L., and Zhao, S. Y.: Atmospheric aerosols and their climatological effect, China  
878 Meteorological Press, Beijing, China, ISBN: 978-7-5029-6676-8, 2017.

879 Zhao, C., Lin, Y., Wu, F., Wang, Y., Li, Z., Rosenfeld, D., and Wang, Y.: Enlarging rainfall area of tropical  
880 cyclones by atmospheric aerosols, *Geophys. Res. Lett.*, 45, 8604-8611,  
881 <http://doi.org/10.1029/2018GL079427>, 2018.

882 Zhao, C. F., Yang, Y. K., Fan, H., Huang, J. P., Fu, Y. F., Zhang, X. Y., Kang, S. C., Cong, Z. Y., Husi, L.,  
883 and Menenti, M.: Aerosol characteristics and impacts on weather and climate over Tibetan Plateau,  
884 *Nat. Sci. Rev.*, 7, 492-495, <http://doi.org/10.1093/nsr/nwz184>, 2020.

885 Zhu, L., Meng, Z., Zhang, F., and Markowski, P. M.: The influence of sea- and land-breeze circulations  
886 on the diurnal variability in precipitation over a tropical island, *Atmos. Chem. Phys.*, 17, 13213–  
887 13232, <https://doi.org/10.5194/acp-17-13213-2017>, 2017.

888 **Figures and tables**

889 Table 1: Summary of information for the verification of OE-SLB at Brisbane Archerfield.

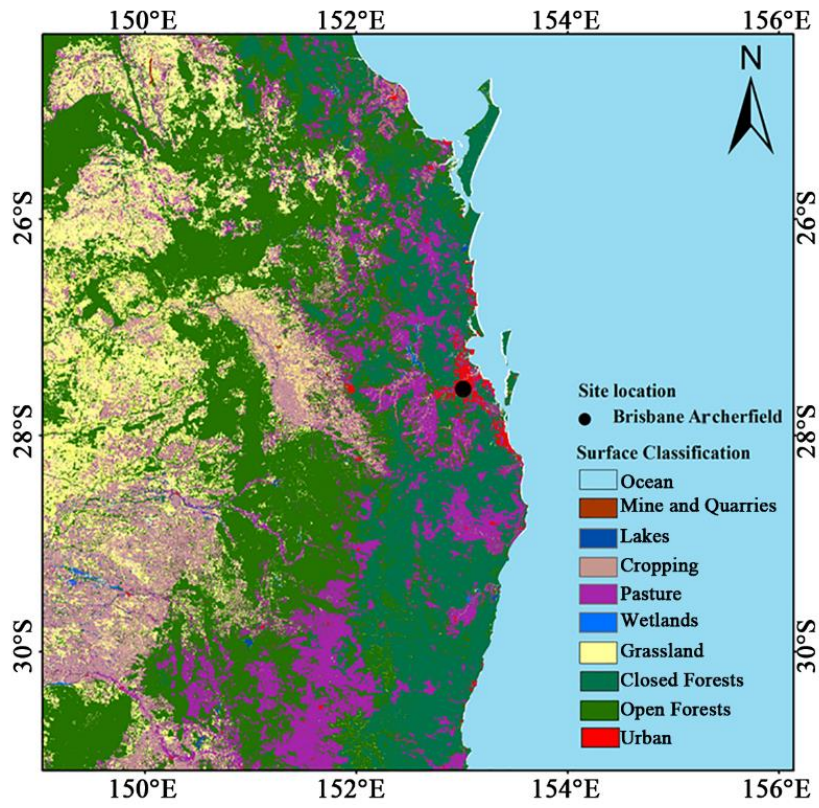
The range of SW	The range of LW	PTS (UTC)	PTL (UTC)
[20° 135°]	[200° 315°]	[500 800]	[1400 2000]

890

891 Table 2: Summary on the effect of different factors on TDLS. Factors marked in red represent that they  
892 are either weak factor or potential factor derived from theoretical analysis but not verified by observation.

Influencing factors	Forcing on Daytime	Forcing on Nighttime	
	TDLS	TDLS	
Large scale forcing	Cooling of SST on a large scale (Hirsch and Koren, 2021)	+	-
Regional forcing	Heating effect of nearby fire spots	+	-
	Total aerosols	-	×
	BC	+	-
	OC	-	×

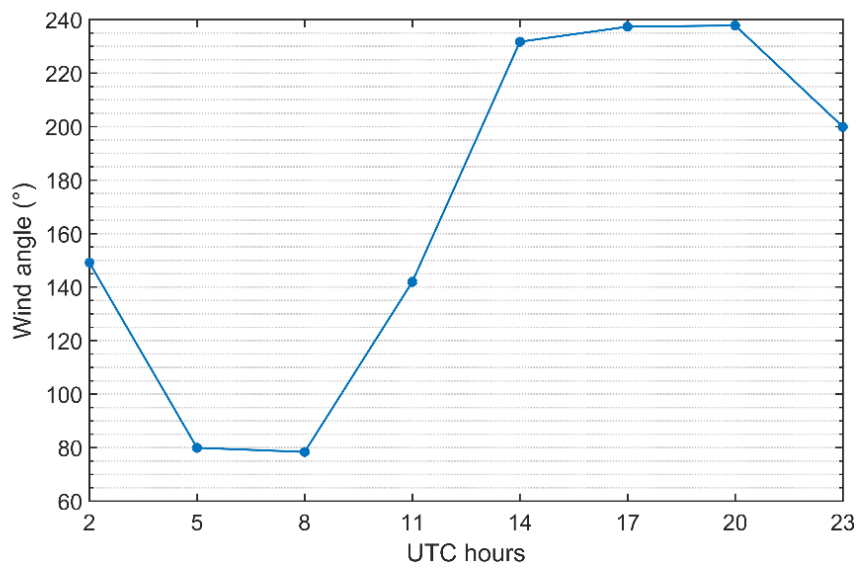
893



894

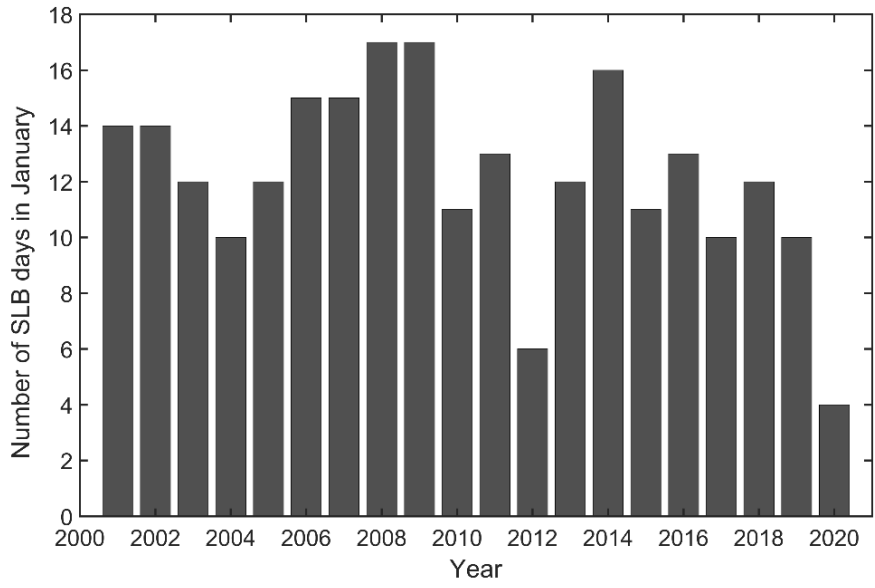
895 Figure 1: The map of eastern Australia with land-cover types. The observation site is marked in a black

896 dot.



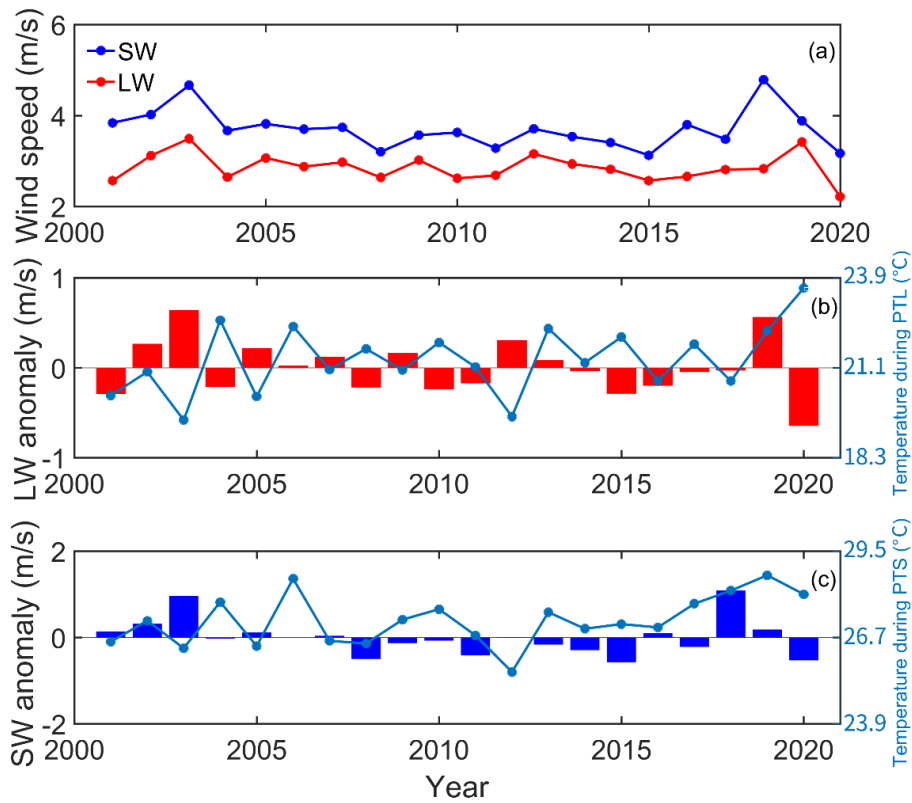
897

898 Figure 2: Hourly average of wind angle in a diurnal period (HAWADP) of the local wind.



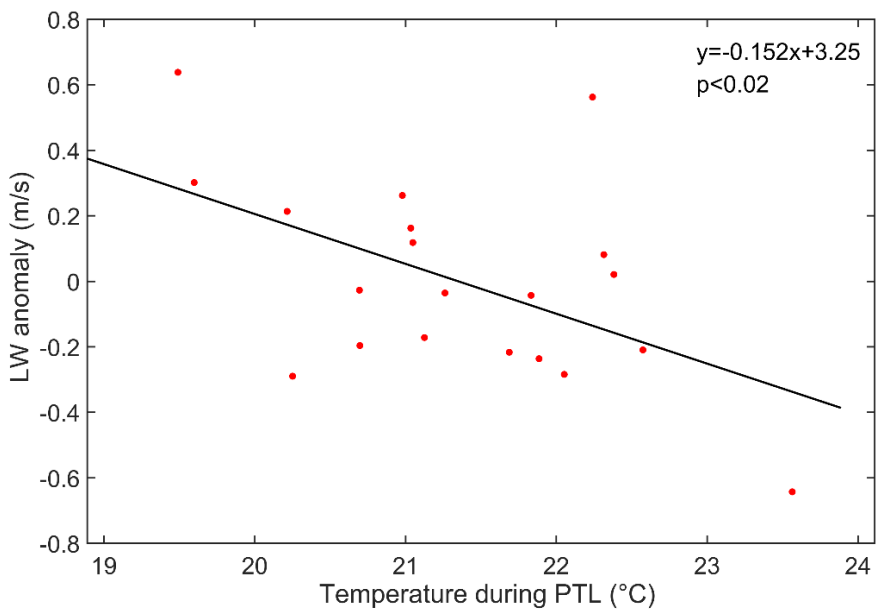
899

900 Figure 3: Number of SLB days in January from 2001 to 2020.

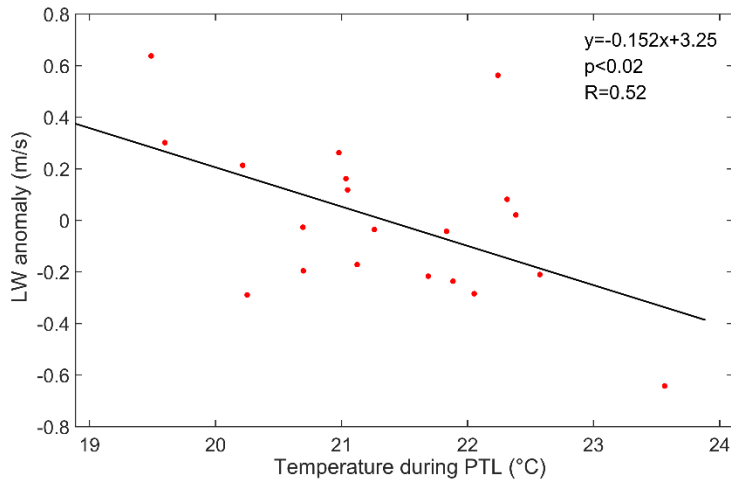


901

902 Figure 4: The trends of SW and LW speeds (a), the LW speed anomaly and land temperature during  
 903 nighttime (b), the SW speed anomaly and land temperature during daytime (c) based on the monthly  
 904 average of them during January from 2001 to 2020.

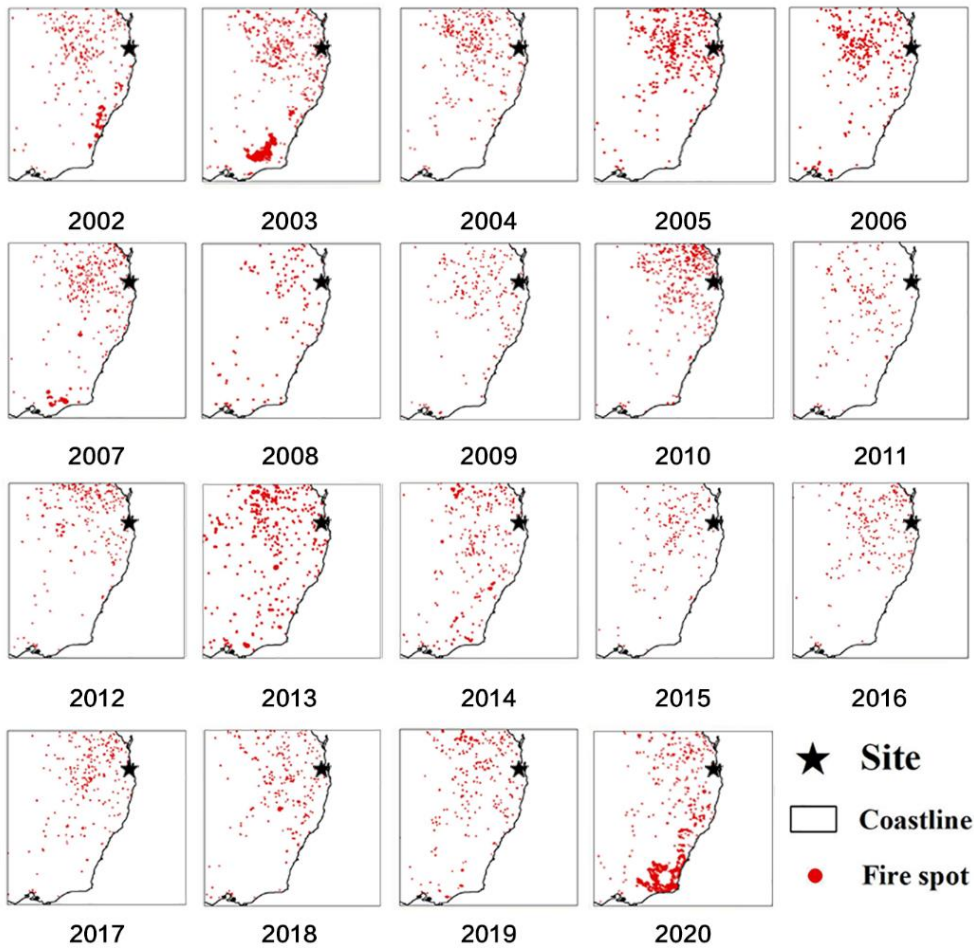


905



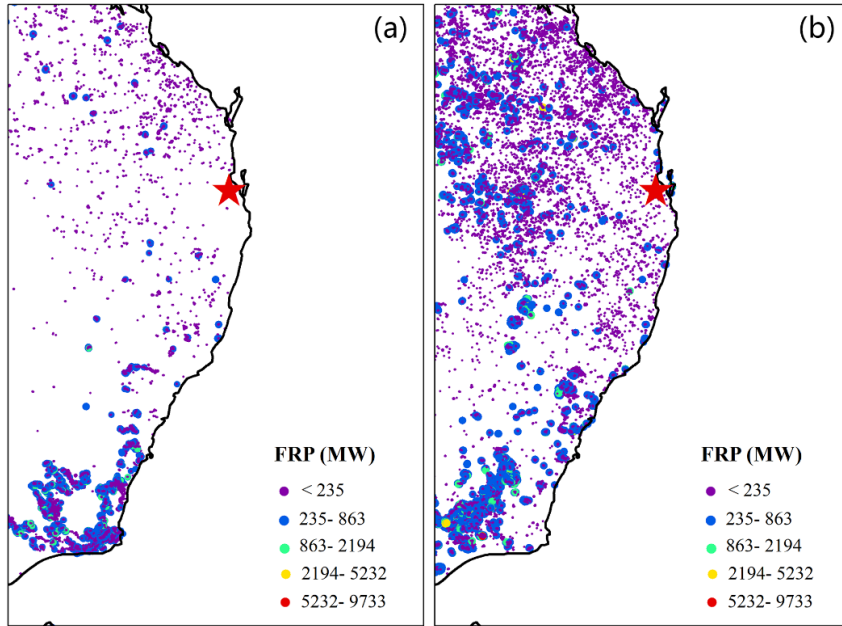
906

907 Figure 5: The relationship between LW anomaly and temperature during PTL based on monthly average  
 908 of them during January from 2001 to 2020.



909

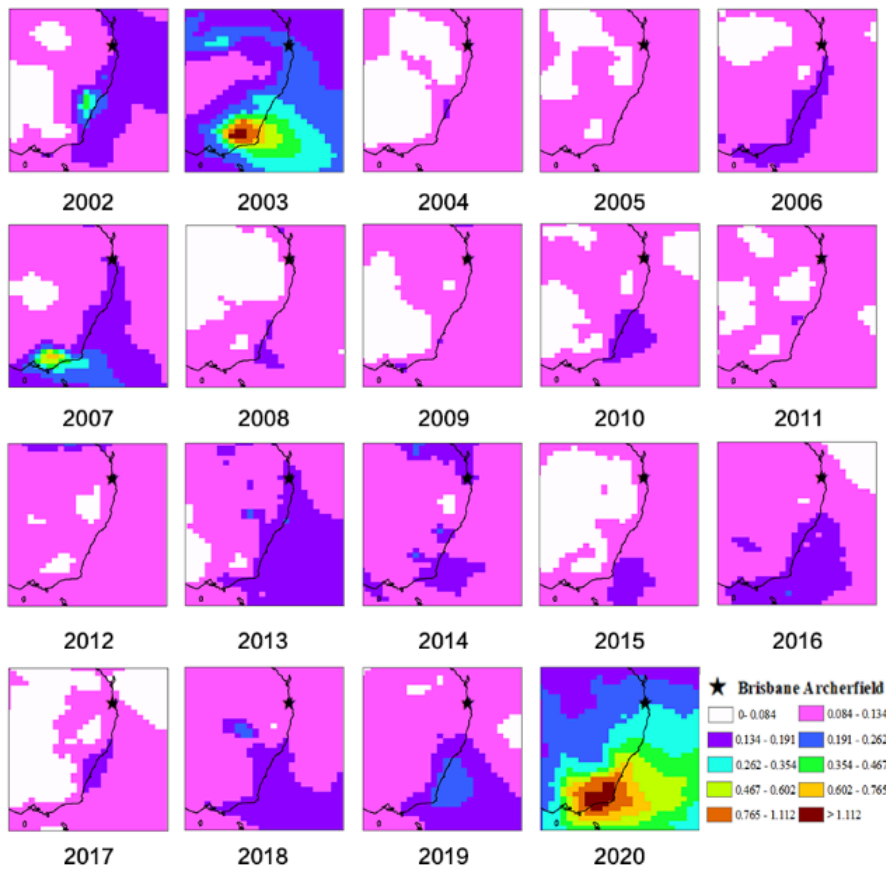
910 Figure 6: The fire spot distribution in the eastern Australia during January from 2002 to 2020.



911

912 Figure 7: The fire radiative power (FRP) of total fire spots in eastern Australia during January in 2020

913 (a), January from 2002 to 2019 (b).



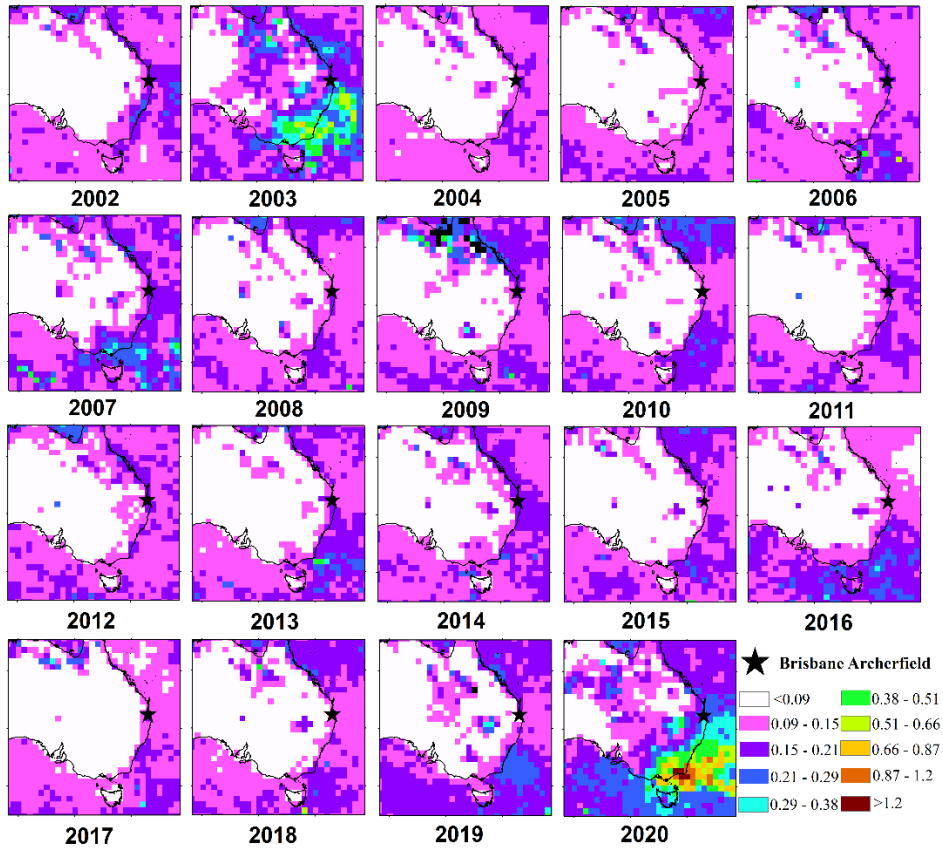
914

915 Figure 8: The spatial distribution of aerosol optical depth (AOD) of total aerosols in eastern Australia

916 during January from 2002 to 2020 [using Modern-Era Retrospective analysis for Research and](#)

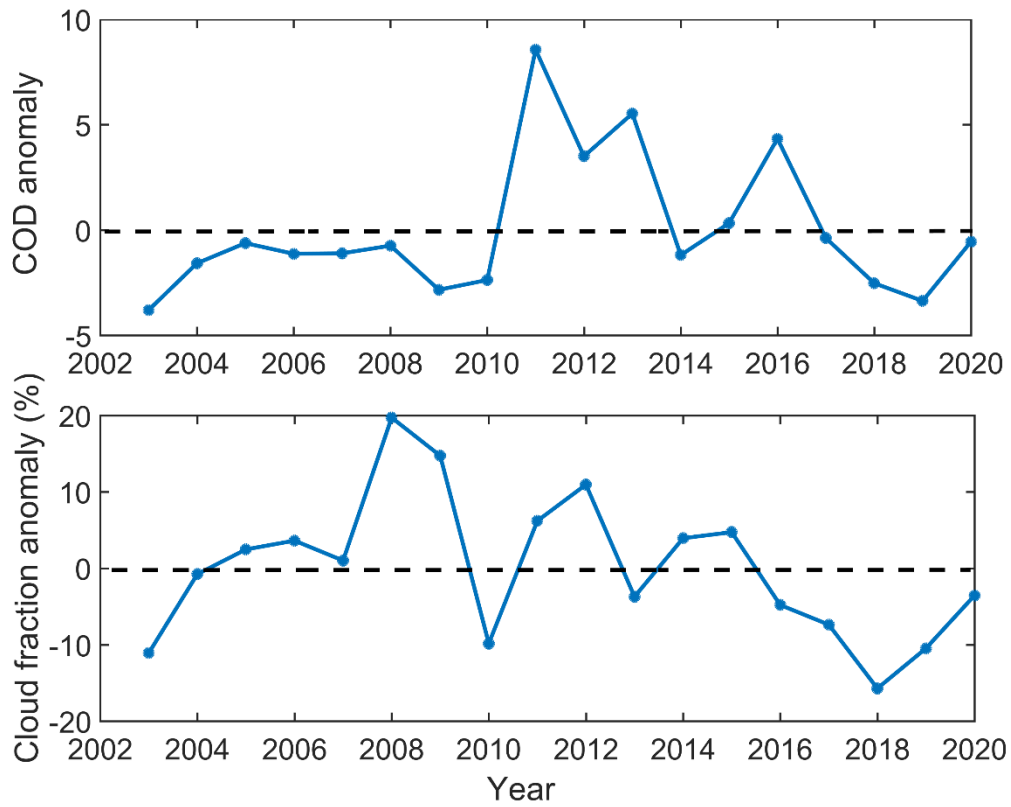
917 [Applications version 2 \(MERRA-2\) AOD product.](#)

918 \_\_\_\_\_



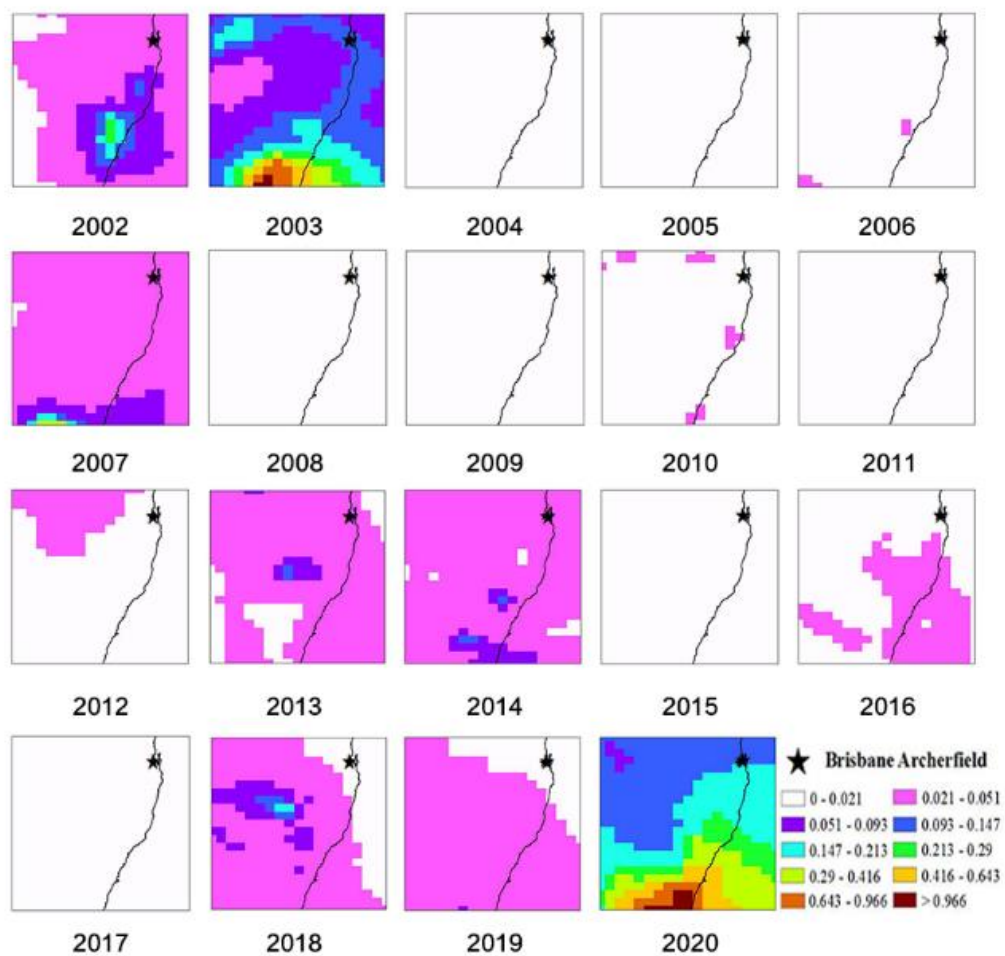
919

920 Figure 9: The spatial distribution of aerosol optical depth (AOD) of total aerosols in eastern Australia  
 921 during January from 2002 to 2020 using Moderate Resolution Imaging Spectroradiometer (MODIS)  
 922 AOD product.



923

924 Figure 109: The monthly cloud optical depth (COD) anomaly and cloud fraction anomaly at Brisbane  
 925 Archerfield during January from 2003 to 2020.



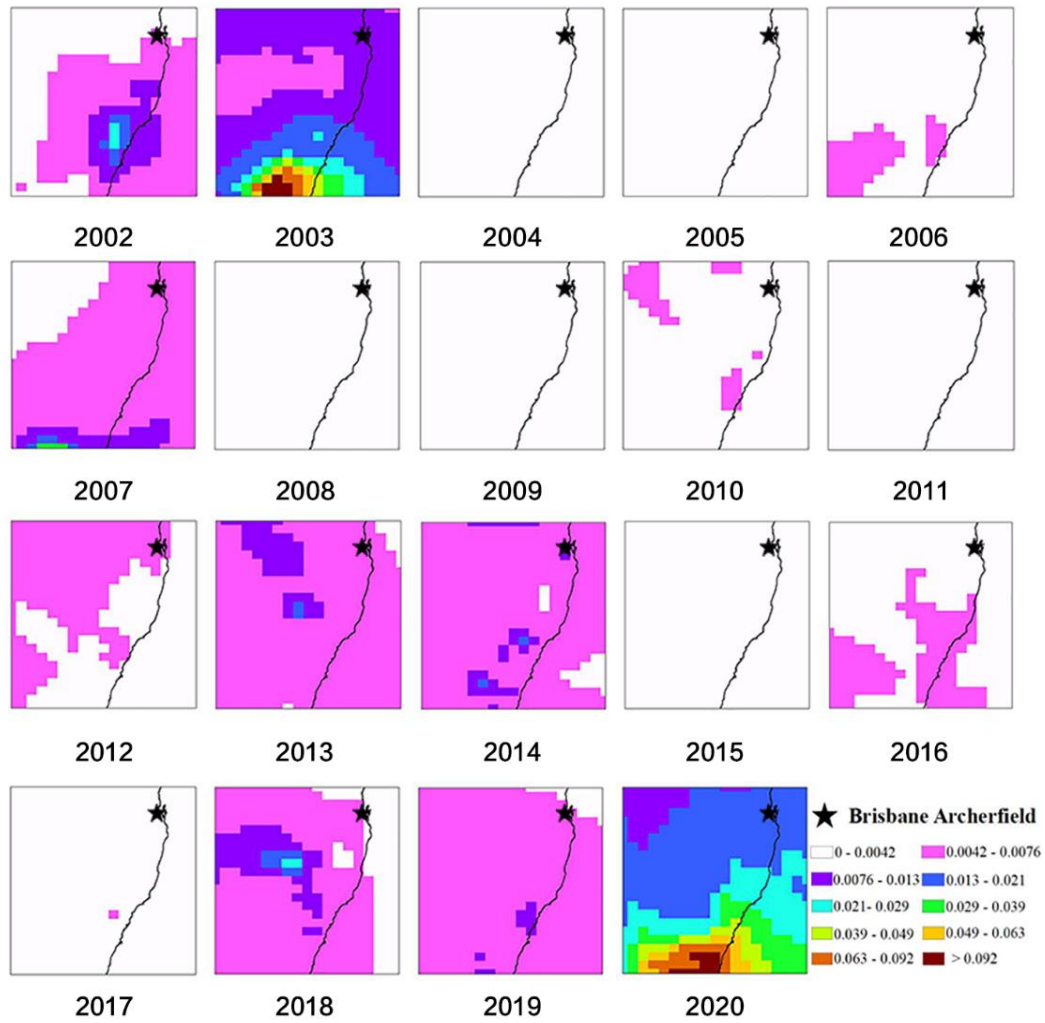
926

927

Figure 119: The spatial distribution of aerosol optical depth (AOD) of organic carbon (OC) in eastern

928

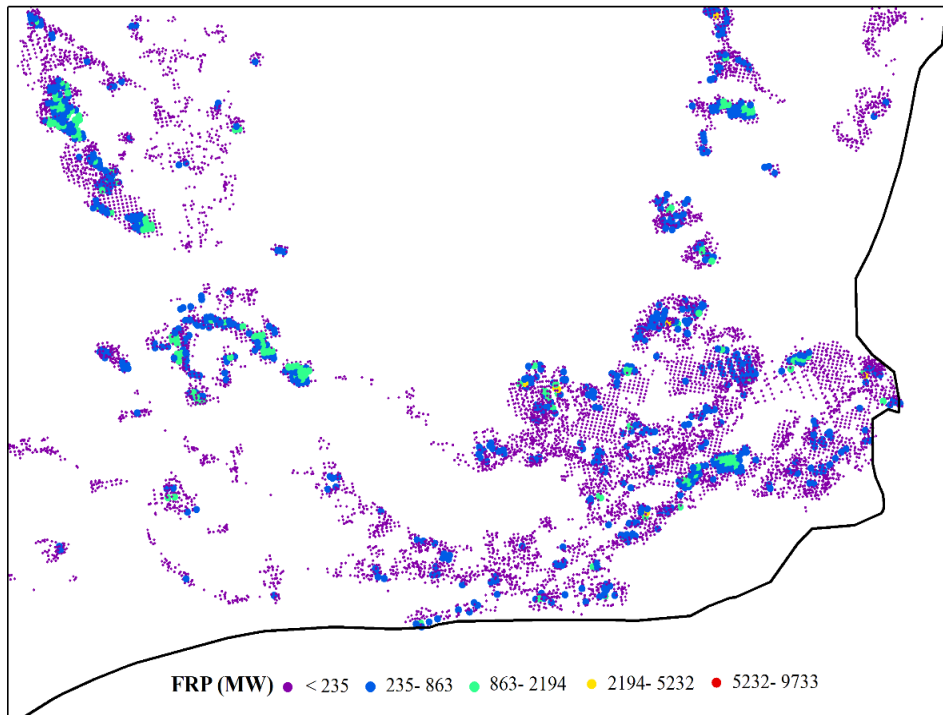
Australia during January from 2002 to 2020.



929

930 Figure 124: The spatial distribution of aerosol optical depth (AOD) of black carbon (BC) in eastern

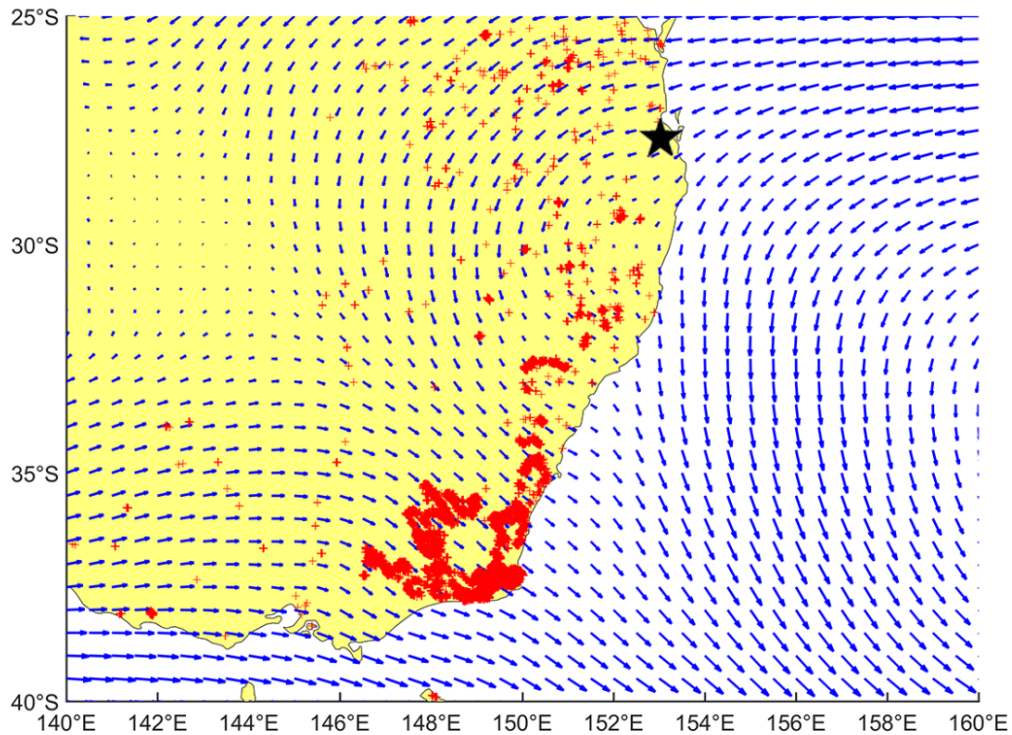
931 Australia during January from 2002 to 2020.



932

933

Figure 132: The detailed distribution of fire spots and their FRP in the fire center during January in 2020.



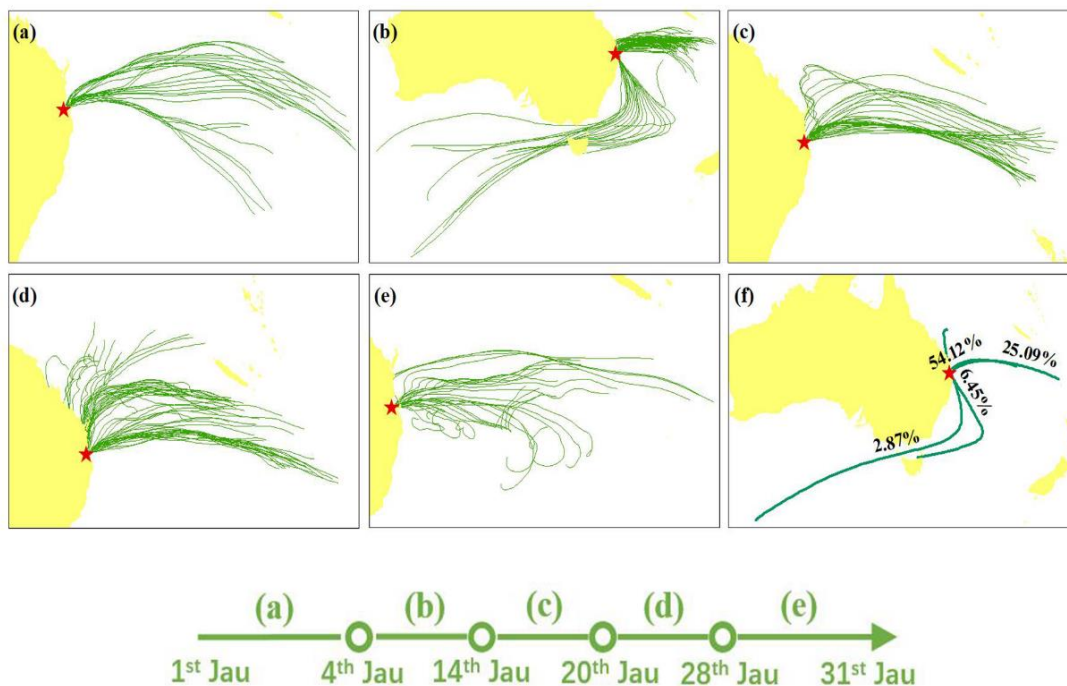
934

935

936

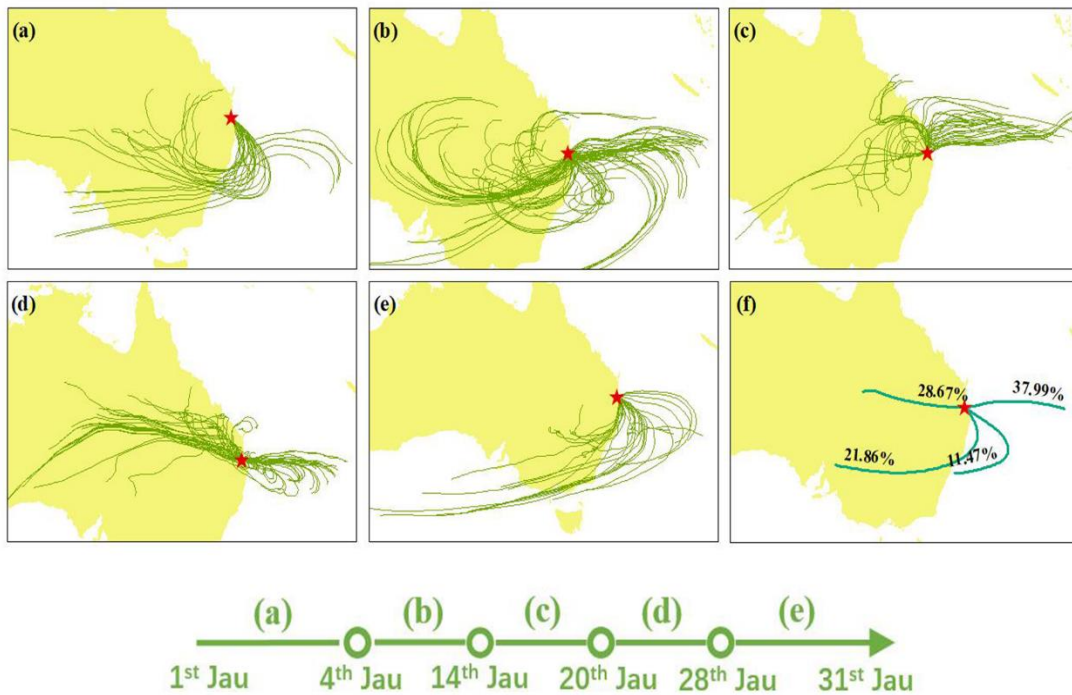
937

Figure 143: Monthly average background wind field based on wind information at pressure levels from 100hPa to 700hPa in January of 2020. The red crosses present fire spots and the black star represents the site location.



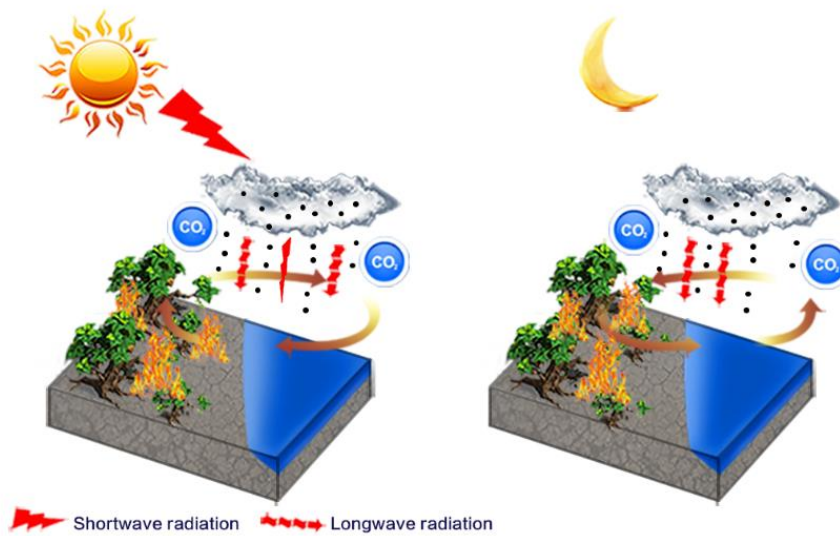
938

939 Figure 154: The site's the wind backward trajectories at 500 m during January in 2020. The wind  
 940 backward trajectories during first No-SLB period from 1st Jau to 3th Jau (a), the wind backward  
 941 trajectories during second No-SLB period from 5th Jau to 13th Jau (b), the wind backward trajectories  
 942 during third No-SLB period from 15th Jau to 19th Jau (c), the wind backward trajectories during fourth  
 943 No-SLB period from 21st Jau to 27th Jau (d), the wind backward trajectories during fifth No-SLB period  
 944 from 29th Jau to 31st Jau (e), the contribution of four main wind clusters based on the wind backward  
 945 trajectories during the whole month of January in 2020 (f).

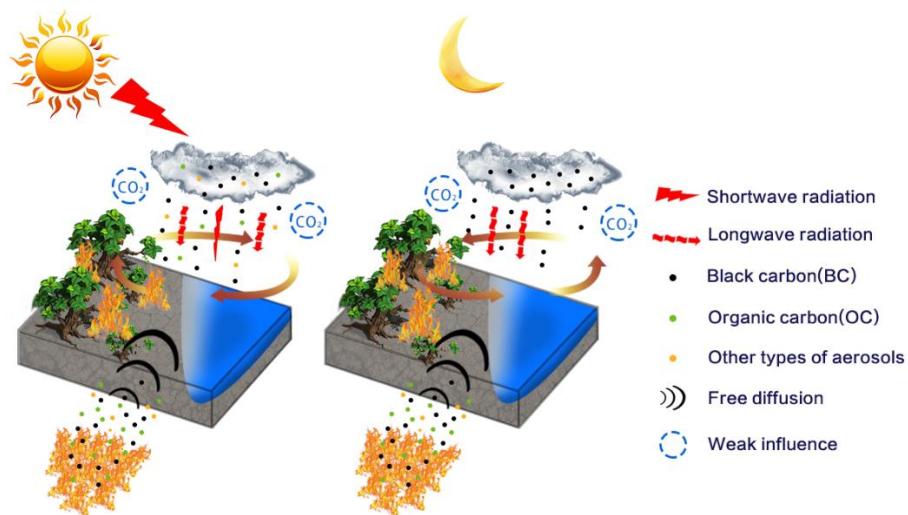


946

947 Figure 165: The site's the wind backward trajectories at 3 km during January in 2020. The wind backward  
 948 trajectories during first No-SLB period from 1st Jau to 3th Jau (a), the wind backward trajectories during  
 949 second No-SLB period from 5th Jau to 13th Jau (b), the wind backward trajectories during third No-SLB  
 950 period from 15th Jau to 19th Jau (c), the wind backward trajectories during fourth No-SLB period from  
 951 21st Jau to 27th Jau (d), the wind backward trajectories during fifth No-SLB period from 29th Jau to 31st  
 952 Jau (e), the contribution of four main wind clusters based on the wind backward trajectories during the  
 953 whole month of January in 2020 (f).



954



955

956 Figure 176: The summary of mechanisms containing influencing factors of local SLB during daytime  
 957 and nighttime. The larger fire cluster represents the center of mega fires with a higher concentration of  
 958 all types of aerosols. During Australia mega fires, aerosols were transported to the local site by means of  
 959 free diffusion, which was caused by the great concentration gap of aerosols between fire center and the  
 960 local site. The black dots represent aerosols which include both scattering aerosols and absorptive  
 961 aerosols. The width of arrows of 'shortwave radiation' represents the magnitude of shortwave radiation.